Cell Reports
Medicine

Article

# Estrogen-related receptor alpha drives mitochondrial biogenesis and resistance to neoadjuvant chemoradiation in esophageal cancer

## Graphical abstract

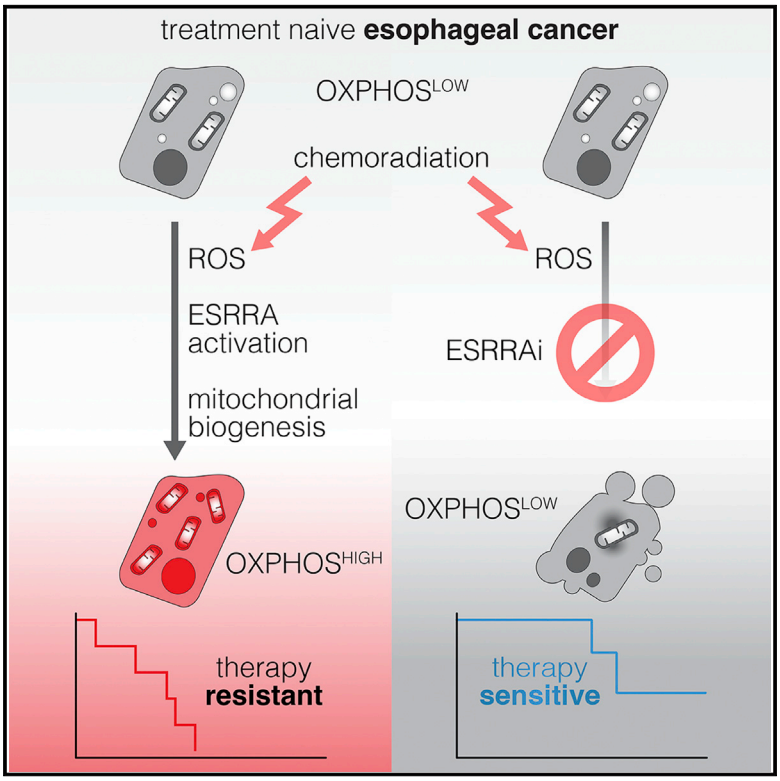


## Authors

Mark P.G. Dings, Amber P. van der Zalm, Sanne Bootsma, ..., Jan Paul Medema, Hanneke W.M. van Laarhoven, Maarten F. Bijlsma

## Correspondence

m.f.bijlsma@amsterdamumc.nl

## In brief

Dings et al. describe a novel metabolic rewiring in esophageal cancers treated with chemoradiation. Estrogen-related receptor alpha was identified as the mediator of an increased mitochondrial respiration following treatment, which conferred resistance. Inhibition of estrogen-related receptor alpha sensitizes cancer cells to (chemo) radiation in preclinical models for esophageal adenocarcinoma.

## Highlights

- Irradiated esophageal cancers upregulate oxidative phosphorylation components
- ESRRA is activated by ROS and drives mitochondrial biogenesis
- Inhibition of ESRRA sensitizes preclinical esophageal cancer models to radiation

Dings et al., 2022, Cell Reports Medicine *3*, 100802
November 15, 2022 
https://doi.org/10.1016/j.xcrm.2022.100802

CellPress

Cell Reports Medicine

CellPress
OPEN ACCESS

Article

# Estrogen-related receptor alpha drives mitochondrial biogenesis and resistance to neoadjuvant chemoradiation in esophageal cancer

Mark P.G. Dings,[1,2,3,11] Amber P. van der Zalm,[1,3,11] Sanne Bootsma,[1,2,3] Tatum F.J. van Maanen,[1,3] Cynthia Waasdorp,[1,2,3] Tom van den Ende,[1,3,4] Dajia Liu,[1,3,4] Peter Bailey,[5] Jan Koster,[1,3] Danny A. Zwijnenburg,[1,3] C. Arnold Spek,[1,3] Jan P.G. Klomp,[6] Arthur Oubrie,[6] Gerrit K.J. Hooijer,[7] Sybren L. Meijer,[7] Mark I. van Berge Henegouwen,[8] Maarten C. Hulshof,[9] Jacques Bergman,[10] Cesar Oyarce,[1,3,4] Jan Paul Medema,[1,2,3] Hanneke W.M. van Laarhoven,[3,4,12] and Maarten F. Bijlsma[1,2,3,12,13,*]

[1]Amsterdam UMC Location University of Amsterdam, Center for Experimental and Molecular Medicine, Laboratory of Experimental Oncology and Radiobiology, Meibergdreef 9, 1105 AZ Amsterdam, the Netherlands
[2]Oncode Institute, Amsterdam, the Netherlands
[3]Cancer Center Amsterdam, Cancer Biology, Amsterdam, the Netherlands
[4]Amsterdam UMC Location University of Amsterdam, Department of Medical Oncology, Amsterdam, the Netherlands
[5]School of Cancer Sciences, University of Glasgow, Glasgow, UK
[6]Lead Pharma, Oss, the Netherlands
[7]Amsterdam UMC Location University of Amsterdam, Department of Pathology, Amsterdam, the Netherlands
[8]Amsterdam UMC Location University of Amsterdam, Department of Surgery, Amsterdam, the Netherlands
[9]Amsterdam UMC Location University of Amsterdam, Department of Radiotherapy, Amsterdam, the Netherlands
[10]Amsterdam UMC Location University of Amsterdam, Department of Gastroenterology, Amsterdam, the Netherlands
[11]These authors contributed equally
[12]Senior author
[13]Lead contact
*Correspondence: m.f.bijlsma@amsterdamumc.nl
https://doi.org/10.1016/j.xcrm.2022.100802

## SUMMARY

Neoadjuvant chemoradiotherapy (nCRT) improves outcomes in resectable esophageal adenocarcinoma (EAC), but acquired resistance precludes long-term efficacy. Here, we delineate these resistance mechanisms. RNA sequencing on matched patient samples obtained pre-and post-neoadjuvant treatment reveal that oxidative phosphorylation was the most upregulated of all biological programs following nCRT. Analysis of patient-derived models confirms that mitochondrial content and oxygen consumption strongly increase in response to nCRT and that ionizing radiation is the causative agent. Bioinformatics identifies estrogen-related receptor alpha (ESRRA) as the transcription factor responsible for reprogramming, and overexpression and silencing of ESRRA functionally confirm that its downstream metabolic rewiring contributes to resistance. Pharmacological inhibition of ESRRA successfully sensitizes EAC organoids and patient-derived xenografts to radiation. In conclusion, we report a profound metabolic rewiring following chemoradiation and demonstrate that its inhibition resensitizes EAC cells to radiation. These findings hold broader relevance for other cancer types treated with radiation as well.

## INTRODUCTION

Over the last 50 years, the incidence of esophageal adenocarcinoma (EAC) has increased steadily in Western countries.[1] For patients eligible for surgery, the standard of care in many countries includes neoadjuvant chemoradiation therapy (nCRT) according to the CROSS regimen.[2,3] Patients who receive neoadjuvant treatment have a 10-year overall survival of 38% compared with 25% for those that receive surgery only.[4] Despite the improvement in survival, long-term outcomes of esophageal cancer remain poor, and many patients who initially respond to multimodality treatment will develop local or distant recurrence.[3,5]

One of the leading factors to preclude complete curative treatment of EAC is a high degree of plasticity of these cancer cells. Therapeutic pressure can cause acquired resistance to occur rapidly, and endows the remaining cells with increased metastatic capacity. Previously identified mechanisms of acquired resistance include the upregulation of compensatory receptor tyrosine kinase signaling in response to targeted therapies,[6] and the induction of epithelial-to-mesenchymal transition (EMT) in response to stromal IL-6.[7] Of note, chemoradiation

(CR) was also found to induce resistance by driving the expression of TGF-β, and subsequent EMT in EAC cells.[8] From the above considerations it is apparent that therapeutic regimens that do not efficiently kill EAC cells are likely to induce therapy-induced resistance. Novel (targeted) therapies are thus required to boost the efficacy of currently used treatment modalities.

Cancer cells are known to employ metabolic pathways that are not favored in non-tumor tissue.[9,10] Traditionally, this has included aerobic glycolysis rather than oxidative phosphorylation to generate ATP from glucose, but it is now apparent that cancer cells harbor a remarkable flexibility that can affect all aspects of cellular metabolism.[11] This flexibility is required not only to meet nutritional challenges at the site of cancer growth, but also to deal with therapeutic stressors such as chemotherapy. Several studies have shown that cancer metabolism contributes to drug resistance, but none have yet investigated the metabolic mechanisms of neoadjuvant chemoradiotherapy resistance in the esophagus.

To achieve a comprehensive overview of the changes in tumor cell biology that occur during nCRT in EAC, we here performed a transcriptomic assessment of a set of pre- and post-treatment patient tissue samples. This identified a marked upregulation of mitochondrial gene expression and associated oxidative phosphorylation. This was confirmed in patient-derived primary cultures exposed to an *in vitro* approximation of the CROSS regimen. Targeting this mitochondrial biogenesis response using pharmacological and genetic methods rendered patient-derived EAC models, including organoids and xenografts, sensitive to (chemo)radiation. We propose that the inhibition of resistance-associated metabolic pathways in addition to (chemo)radiation is a promising modality for the treatment of EAC.

## RESULTS

### Esophageal carcinomas exposed to neoadjuvant CR upregulate oxidative phosphorylation components

The standard of care for resectable esophageal cancer (both for EAC and squamous cell carcinoma [ESC]) is nCRT according to the CROSS regimen. However, responses to this neoadjuvant treatment vary considerably between patients and resistance mechanisms are at play that hamper therapeutic efficacy. We aimed to identify such mechanisms by gene expression analysis of pre- and post-treatment samples of both EAC and ESC. In a cohort of pre-treatment biopsies and resection specimens from our institute, six matched samples were identified from patients who underwent nCRT followed by resection, and of whom the samples were of sufficient quality for next-generation sequencing (Figure 1A; baseline characteristics in Table S1). RNA-seq was performed, and gene set enrichment analysis (GSEA)[12] including all Hallmark gene signatures revealed a marked upregulation of genes involved in oxidative phosphorylation in post-treatment samples (Figure 1B, inset). The increase in oxidative phosphorylation was not confounded by changes in tumor cellularity and was also observed if only EAC samples were considered (excluding ESC; Figures S1B–S1D). Of note, principal-component analysis revealed that treatment effect explained most of the variance, and not histology (Figure S1D). The upregulation in response to nCRT was seen across all oxidative phosphorylation complexes (Figure 1C), and in all but one patient (Figure S1E).

In addition to these gene expression analyses, immunohistochemical staining for cytochrome C oxidase subunit 4 (a constituent of complex IV and general marker for mitochondria) was performed in paraffin embedded patient samples that were largely non-overlapping with the initial RNA-seq analysis (Figures 1D and 1E; baseline characteristics in Table S2; included sample IDs in Table S3). These data support the notion that post-CR esophageal cancers have increased mitochondrial content.

### CR increases mitochondrial content and oxygen consumption in EAC cells

To functionally characterize the metabolic response to CR at the cellular level in EAC specifically, we treated publicly available as well as primary patient-derived EAC cell lines to an *in vitro* approximation of the CROSS regimen (see STAR Methods for details).[8] Analysis of baseline oxygen consumption rate over extracellular acidification rate (ECAR) (a measure of lactate production through glycolysis) by Seahorse flux analysis showed a clear shift in bioenergetic flux toward oxidative phosphorylation following CR in almost all esophageal cell lines (Figure 2A). Mitochondrial stress testing revealed that respiration was increased, in particular maximal respiration (Figures 2B and 2C). Conversely, basal ECAR levels and measurements of glycolysis pathway transcripts showed a reduction in response to CR (Figures S2A and S2B). Confocal microscopy of dye-labeled mitochondria in treatment naive and chemoradiated 289B cells showed an increase of mitochondrial content in treated cells (Figure 2D). This was also found by transmission electron microscopy (Figure 2E, high magnifications of mitochondrial morphology shown in Figure S2C). Of note, surviving cells showed an altered morphology, as reported by us previously.[8] Therefore, to correct for changes in cell mass or density, mitochondrial DNA copy numbers normalized to cellular genomic DNA were measured in parallel. This confirmed the upregulation of mitochondria (Figure 2F) and was observed across a panel of EAC cell lines exposed to CR (Figure S2D). Together, these results point to a robust cellular reprogramming in response to CR resulting in an upregulation of cellular respiration.

### Reactive oxygen species generated in response to ionizing radiation drive mitochondrial biogenesis

To identify which of the components of the CR regimen drives the increased mitochondrial respiration, we exposed EAC cells to chemotherapy, radiation, or the combination, and measured mitochondrial content using a fluorescent dye (Figure S2E). Radiation alone was found to be sufficient to increase mitochondrial content. Indeed, it is known that exposure to radiation, and to a lesser extent chemotherapy, induces reactive oxygen species (ROS).[13] In turn, mitochondria are key regulators of ROS levels,[14] and we investigated this interconnection by measurements and perturbations of ROS. ROS were measured using a chemical probe and we observed that brief exposure to ionizing radiation induces ROS levels that approach those resulting from long-term CR (Figure S2F). This indicates that ROS production from radiation is acute and that this modality of the CR regimen is likely the

CellPress
OPEN ACCESS

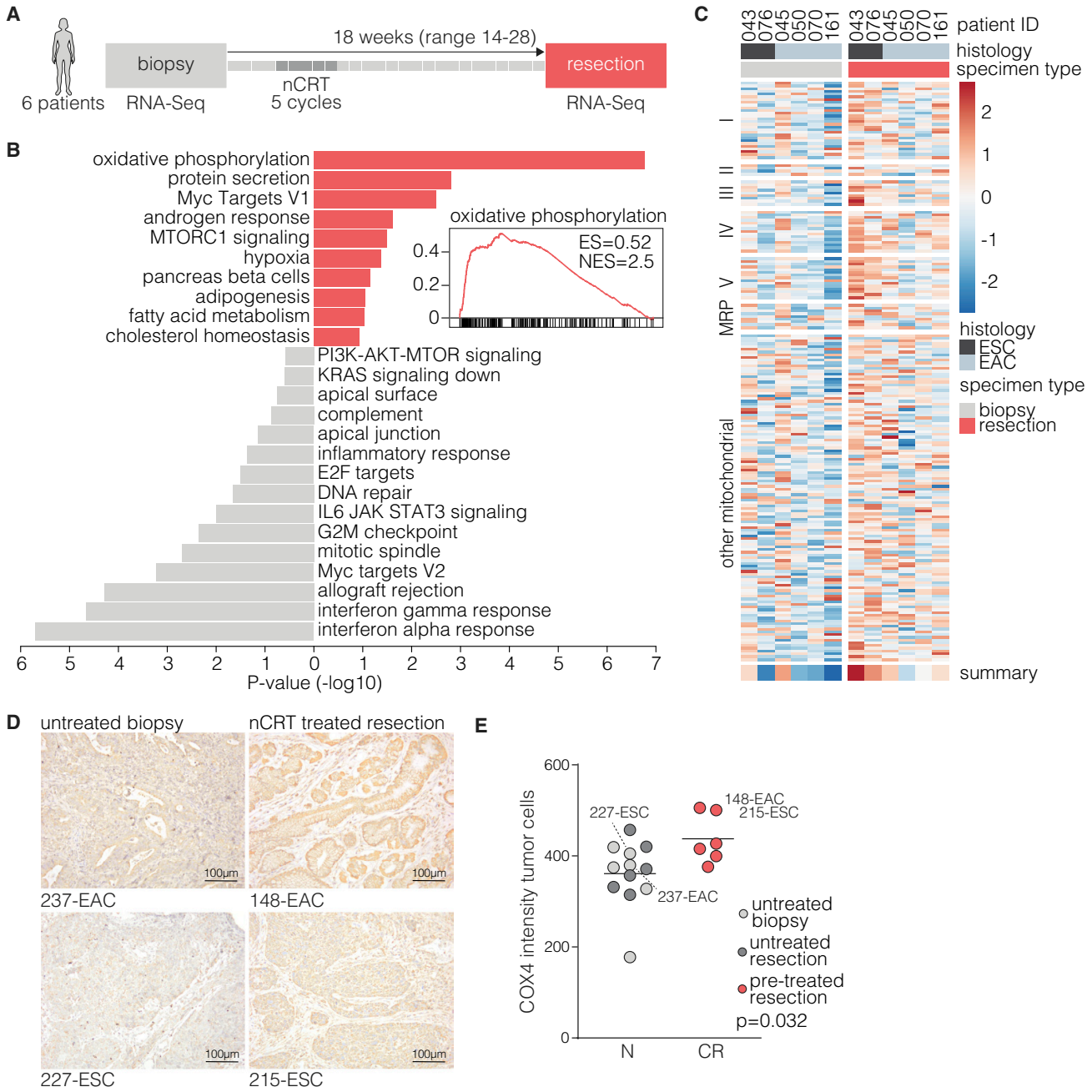


**Figure 1. Expression of oxidative phosphorylation components in patient samples following neoadjuvant chemoradiation**

(A) Diagram of analyzed samples. Squares indicate weeks between biopsy and resection, dark gray blocks indicate nCRT cycles according to CROSS: five cycles of neoadjuvant chemoradiotherapy were given: radiotherapy in 23 fractions of 1.8 Gy on 5 days per week (totaling 41.4 Gy), with concurrent carboplatin at AUC 2 mg/mL per min, and paclitaxel at 50 mg/m$^2$ body surface followed by surgery. Average time between pre-treatment biopsy and resection is indicated with range parenthesized.

(B) Gene set enrichment analyses were performed using indicated MSigDB Hallmark gene sets. Shown is significance of association with treatment naive biopsies (gray) and neoadjuvant chemoradiated resection specimens (red). Inset shows GSEA curve for oxidative phosphorylation gene set. Resection specimens are left on the phenotype bar.

(C) Heatmap showing relative gene expression across oxidative phosphorylation compartments: complexes I–V, mitochondrial ribosomal proteins (MRP), and other oxidative phosphorylation-related genes.

(D) Immunohistochemistry for cytochrome C oxidase subunit 4 (COX4) was performed on non-matched pre-treatment biopsies and untreated resection specimens and CROSS resection specimens, from EAC and ESC. Scale bar, 500 μm.

(E) Tumor ROIs were annotated by a pathologist, and the intensity of COX4 staining in tumor areas was quantified using ImageJ. Each dot indicates an individual patient sample. Statistical analyses were performed using Mann-Whitney U test.

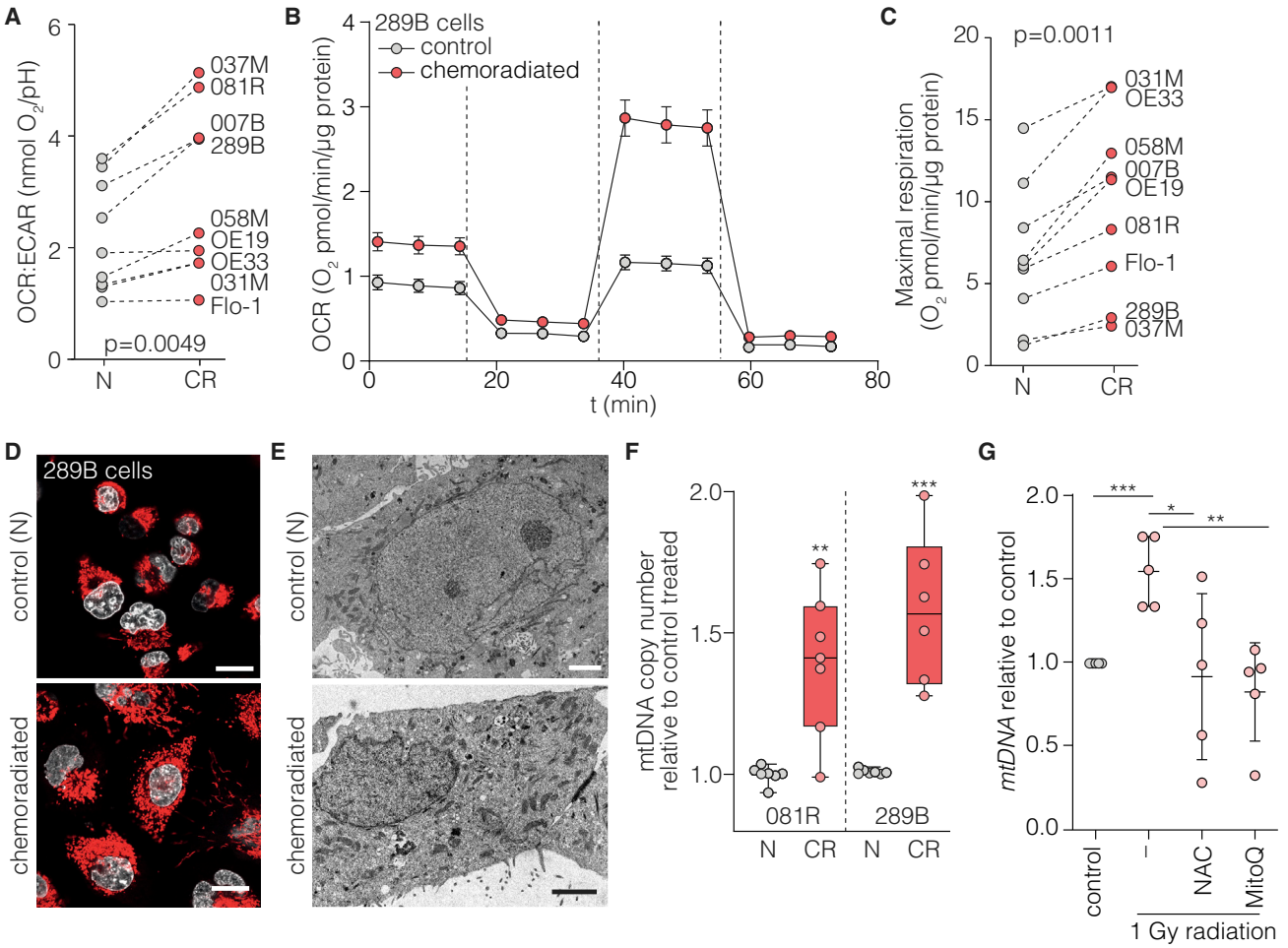


**Figure 2. Metabolic cellular responses to chemoradiation**

(A) Baseline oxygen consumption rate (OCR) and extracellular acidification (ECAR) were measured in 14-day chemoradiated (CR) and treatment naive (N) EC cell lines (007B, 031M, 037M, 081R, 289B, Flo-1, OE19 and OE33) using the Seahorse XF96 Extracellular Flux Analyzer. Shown is mean OCR/ECAR per cell line, statistical test is Wilcoxon signed-rank paired.

(B) Example flux analysis result of mitochondrial stress test in 289B cells, N and CR. Sequential addition of compounds at dashed lines were oligomycin, carbonyl cyanide-p-trifluoromethoxy phenylhydrazone (FCCP), and a combination of rotenone and antimycin. Mean ± SD of five or more biological replicates.

(C) As for (A), showing maximal uncoupled respiration derived from mito stress tests. Shown is mean OCR/ECAR per cell line, statistical test is Wilcoxon signed-rank paired.

(D) MitoTracker Deep Red FM fluorescence staining in 289B cells treated as for (A). Magnification is 64×. Scale bar, 20 μm.

(E) Cells treated as for (A) were processed and contrasted for electron microscopy with uranyl acetate and counterstained with lead citrate. Magnification is 1,900×. Scale bare, 2 μm.

(F) Quantitative PCR analysis for mtDNA copy number of mitochondrial-encoded *mtTL1* over nuclear-encoded *B2M*. Data shown are mean ± SD of seven independent experiments. Unpaired t test, $^{**}p < 0.01$, $^{***}p < 0.001$.

(G) 081R cells were subjected to 1 Gy IR and antioxidants for 72 h. N-acetylcysteine (NAC) was used at 5 mM, MitoQ was used at 300 μM. Quantitative PCR for mtDNA copy number is shown. Data shown are expression corrected for *B2M*, mean ± SD of three independent experiments, relative to untreated control. Unpaired t test, $^{*}p < 0.05$, $^{**}p < 0.01$, $^{***}p < 0.001$.

driver of mitochondrial biogenesis. We then defined the temporal dynamics of mitochondrial upregulation in response to radiation alone, and found that this was achieved within several days (Figure S2G). Next, this time frame was used for perturbation experiments with antioxidants N-acetyl cysteine (NAC), and the mitochondrially targeted MitoQ. These effectively prevented the upregulation of mitochondrial copy numbers, suggesting the ROS induced by ionizing radiation drives the increased mitochondrial response in EAC cells (Figure 2G).

## ESRRA is associated with mitochondrial biogenesis in EAC

Mitochondrial mass and morphology are tightly regulated, and highly dynamic to adequately respond to, for instance, altered energy requirements and cell extrinsic cues. To identify which of the known regulators of mitochondrial biogenesis and dynamics are likely at play in esophageal cancer, their association with oxidative phosphorylation hallmark genes was assessed in three previously established gene expression datasets (Figure 3A).[15–17] This

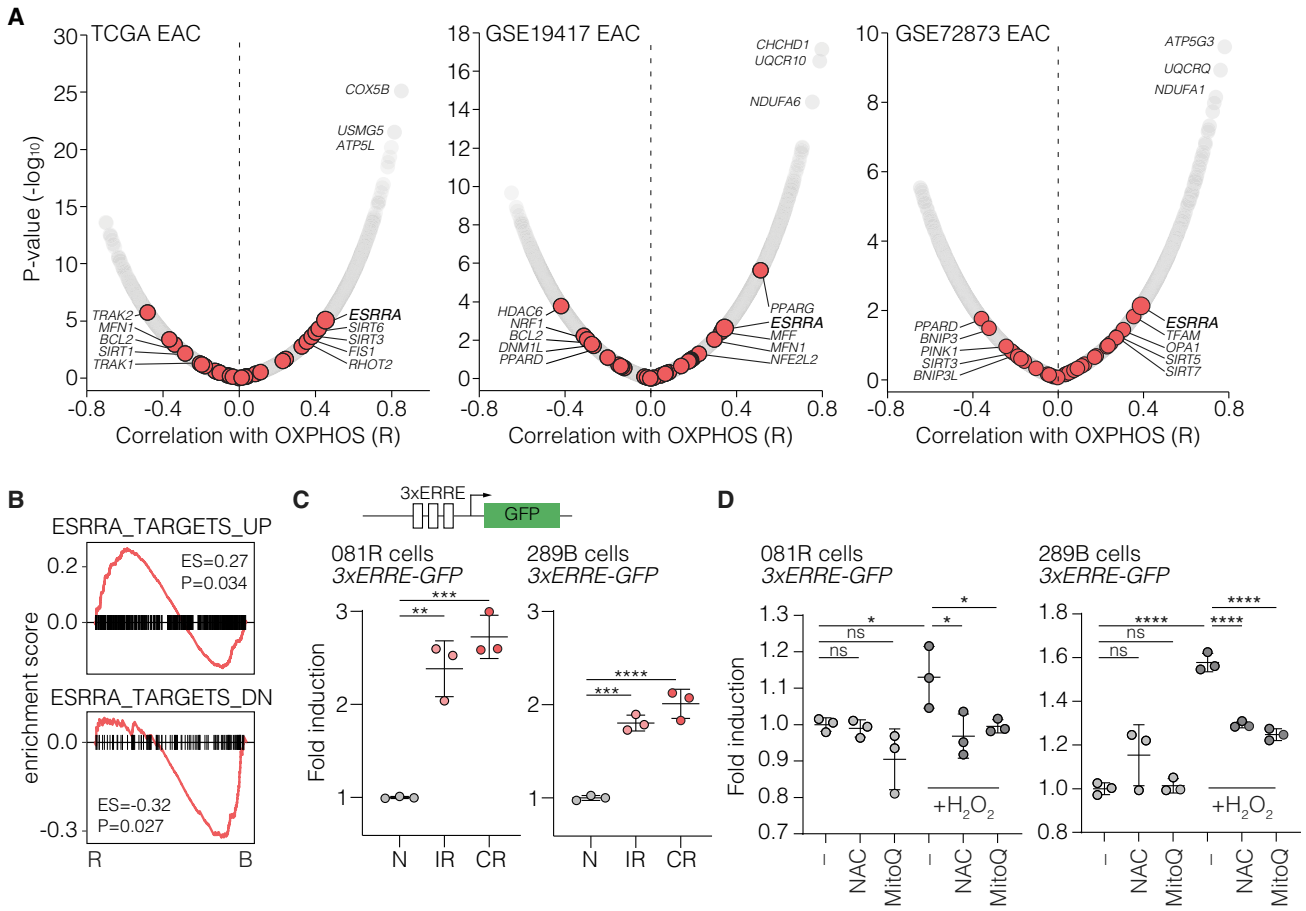


**Figure 3. ESRRA is associated with mitochondrial biogenesis in EAC**

(A) Gene expression correlated to the hallmark oxidative phosphorylation signature (Table S6) using the bioinformatics platform R2.[42] Plotted in volcano plots are correlation coefficients (R) and significances of association (P) of all genes found using the correlate with track function (see also STAR Methods section). Highlighted in red are known regulators of mitochondrial content and dynamics as listed in Table S6. Three previously published sets were analyzed; TCGA_ESCA using EAC samples,[15] GSE19417,[16] GSE72873.[17]

(B) Enrichment of genes that are activated by ESRRA (top), and that are repressed by ESRRA (bottom) by GSEA among genes more highly expressed in neo-adjuvant chemoradiated resection specimens and treatment naive biopsies, respectively. ESs and p values are shown.

(C) Diagram of reporter construct. Indicated ERRE sequence was inserted in the FpG5 reporter plasmid. 081R and 289B cells were transduced with the 3xERRE-GFP reporter, selected for effective transduction, and exposed to radiation or chemoradiation for 14 days. Shown is average gMFI, relative to 0 Gy. Data shown are mean ± SD of three biological replicates. Unpaired t test, $^{**}p < 0.01$, $^{***}p < 0.001$, $^{****}p < 0.0001$.

(D) Indicated ERRE-GFP cells were treated with antioxidants (NAC at 5 mM, MitoQ at 0.3 μM), and 326 mM $H_2O_2$ for 72 h. Analysis of GFP signal and statistics as for (C). Data shown are mean ± SD of three biological replicates. Unpaired one-tailed t test, $^{*}p < 0.05$, $^{**}p < 0.01$, $^{***}p < 0.001$, $^{****}p < 0.0001$.

revealed that estrogen-related receptor alpha (*ESRRA*/ERRα) was most consistently correlated with the expression of oxidative phosphorylation genes. ESRRA is an orphan nuclear receptor which, typically together with coactivators such as peroxisome proliferator-activated receptor gamma coactivator 1-alpha (PGC-1α), regulates mitochondrial content. *ESRRA* transcript levels were found to be similar between the matched pre- and post-nCRT patient samples analyzed by RNA-seq (Figure S3A). In accordance, transcript analysis of *ESRRA* revealed that it was not upregulated in cell lines following CR (Figure S3B), and immunofluorescence in cells exposed to radiation did not reveal a noticeable shift in subcellular localization of ESRRA (Figure S3C). These data suggest that expression-based regulation of *ESRRA* alone does not explain its association with oxidative phosphorylation.

Instead, to assess ESRRA activity rather than its expression levels, we applied GSEA using a published *ESRRA* target gene set (Figure 3B).[18] As expected, post-nCRT resection gene expression was enriched for genes that are activated by *ESRRA*. The opposite was observed for genes known to be suppressed by *ESRRA*, which mainly enriched in pre-nCRT biopsies. These analyses support the notion that *ESRRA* is activated in response to CR and regulates metabolic rewiring.

To formally ascertain that ESRRA is activated in response to (chemo)radiation, we first used a previously published ESRRA luciferase reporter (3x*ERRE*-Luc[19]). HEK293T cells transfected

with this reporter showed a strong activation of ESRRA in response to radiation (Figure S3D). Next, to allow measurements of ESRRA activity in relevant primary EAC models (which are not amenable to transfection) we constructed a reporter system using the same 3x*ERRE* sequences preceding a GFP cassette in a lentiviral transfer vector (3x*ERRE*-GFP*;* diagram in Figure 3C). Indeed, 3x*ERRE*-GFP reporter cells showed a dose-dependent response to radiation within several days (Figures S3E and S3F), and also in response to 14-day radiation or CR (Figure 3C, graphs). Pull-down assays for DNA-bound ESRRA followed by qPCR (for the *SDHA* gene[20]), confirmed that ESRRA directly engages previously identified target gene following CR in EAC cells (Figure S3G). To establish a direct link between ROS and ESRRA activity, we increased ROS levels using $H_2O_2$ in 3x*ERRE*-GFP reporter cells and found that this indeed resulted in increased reporter activity (Figure 3D). This increase could be prevented by the addition of ROS scavengers (NAC and MitoQ).

To functionally demonstrate that ESRRA is not only activated by radiation, but also required for mitochondrial biogenesis in esophageal cancer, we generated isogenic genetic models. We inhibited or overexpressed *ESRRA* by using lentiviral delivery of short hairpin RNAs (shRNAs) or cDNA, respectively. Cells were transduced with shRNAs targeting *ESRRA* or scrambled control and following puromycin selection and validation of knockdown, treated with (chemo)radiation. Knockdown of *ESRRA* largely prevented the upregulation of mitochondrial mass following CR (Figure 4A; knockdown confirmed in Figure S4A). To provide further proof for the functional contributions of ESRRA activity to therapy resistance, EAC cells overexpressing *ESRRA* and a Venus (green) fluorophore were established. This overexpression resulted in an induction of mitochondrial mass comparable to that following CR as expected (Figure 4B; overexpression confirmed in Figure S4B). Following overexpression and silencing of *ESRRA*, transcript levels of a selected set of hallmark regulators of mitochondrial dynamics and biogenesis was measured by qPCR, and this revealed that *ESRRA* likely acts through TFAM (Figure 4C). In accordance, *TFAM* was found to be upregulated in post-treatment resection specimens, as well as in cells exposed to CR *in vitro* (Figures S5A and S5B). These data are in strong agreement with literature describing TFAM as an ESRRA target gene, and the known role of TFAM in promoting mitochondrial genome duplication.[21,22]

The paralogs PPARGC1A and PPARGC1B have been described to function as coactivators of ESRRA.[23–25] We assessed the levels of these genes in the matched patient expression data and did not observe levels to be different between pre- and post-treatment samples (Figure S5C). *In vitro*, expression of these genes did increase following CR (Figure S5D). First, the responsiveness of 3xERRE-GFP reporter to PPARGC1A activity was ascertained (Figure S5E). Next, we knocked down known coactivators of ESRRA (*PPARGC1A/B*). Following knockdown, ESRRA activity was measured at baseline and following radiation (Figure S5F). No reduction in baseline reporter activity was observed, nor was the induction by radiation prevented by knockdown of the ESRRA coactivators *PPARGC1A/B*. We hypothesize that either there is redundancy between the PPARGC1 paralogs and that knocking down one is not effective, or that the PPARGC1 proteins are not required for ESRRA activation in cancer cells exposed to radiation. The increase in expression *in vitro* may suggest that the paralogs indeed function together, or that the CR selects for a PPARGC1-high population.

Together, these data show *ESRRA* to be associated with oxidative phosphorylation in EAC, and although it is not regulated at the transcriptional level or by altered subcellular localization following CR, its activity is strongly increased by radiation-induced ROS and is required for the mitochondrial biogenesis response in this context.

## ESRRA activity contributes to resistance to CR

Given the above findings, we reasoned that inhibition of ESRRA-mediated mitochondrial biogenesis could improve the anti-tumor efficacy of CR. Indeed, exposure of ESRRA-silenced cells to CR and radiation alone revealed these cells to be effectively sensitized to such treatment modalities (Figures 4D, 4E, and S4C). Untreated proliferation rates of shCtrl and sh*ESRRA* were comparable. Next, cells overexpressing *ESRRA* (and the Venus fluorophore) were mixed with control cells and this coculture was exposed to CR. The cells overexpressing ESRRA were found to occupy a much larger surface than wild-type cells did (Figure 4F). Of note, this growth advantage was not observed in control growth conditions in which both populations occupied approximately half the cellular surface area.

These results, the measurements of ESRRA activity, and the bioinformatic analyses lead us to conclude that the presence of ESRRA and its subsequent activation by radiation is required for mitochondrial biogenesis in irradiated EAC tumor cells. In other words, there need to be sufficient levels of ESRRA available for activation by ROS to adequately initiate mitochondrial biogenesis following radiation. The activity of ESRRA, and resultant upregulation of mitochondria, then contributes to resistance in EAC cells.

## Pharmacological inhibition of ESRRA sensitizes cells to CR

Inverse agonist inhibitors of ESRRA have been developed such as 4-[4-(2,4-dioxothiazolidin-5-ylidenemethyl)-2-methoxyphenoxy]-naphthalene-1-carboxylic acid methyl ester, and 4-[4-(2,4-dioxothiazolidin-5-ylidenemethyl)-2-methoxyphenoxy]- 3-trifluoromethylbenzonitrile[26] (ESRRAi). This compound covalently binds ESRRA to alter the confirmation of the AF2 activation domain, preventing binding of coactivator proteins, and blocking cellular responses to increased demands for mitochondrial mass. The approximate $IC_{20}$ of this inhibitor was determined to be around 20 μM in 081R and 289B cells (Figure S6A). At this concentration, ESRRAi prevented both the increase in mitochondrial respiration in response to CR (Figure 5A) and the increase of mitochondrial DNA in response to IR and CR (Figure 5B). Of note, the $IC_{50}$ of ESRRAi in control shRNA transduced cells was 71 μM, which was increased to 129 and 133 μM in cells silenced for *ESRRA*.

We then proceeded to further delineate the cellular responses to CR in the presence of ESRRAi. We observed that the mitochondrial membrane potential (as measured using JC-1) was markedly increased after CR (Figure S6B). This increase in membrane potential could be caused by an insufficient upregulation

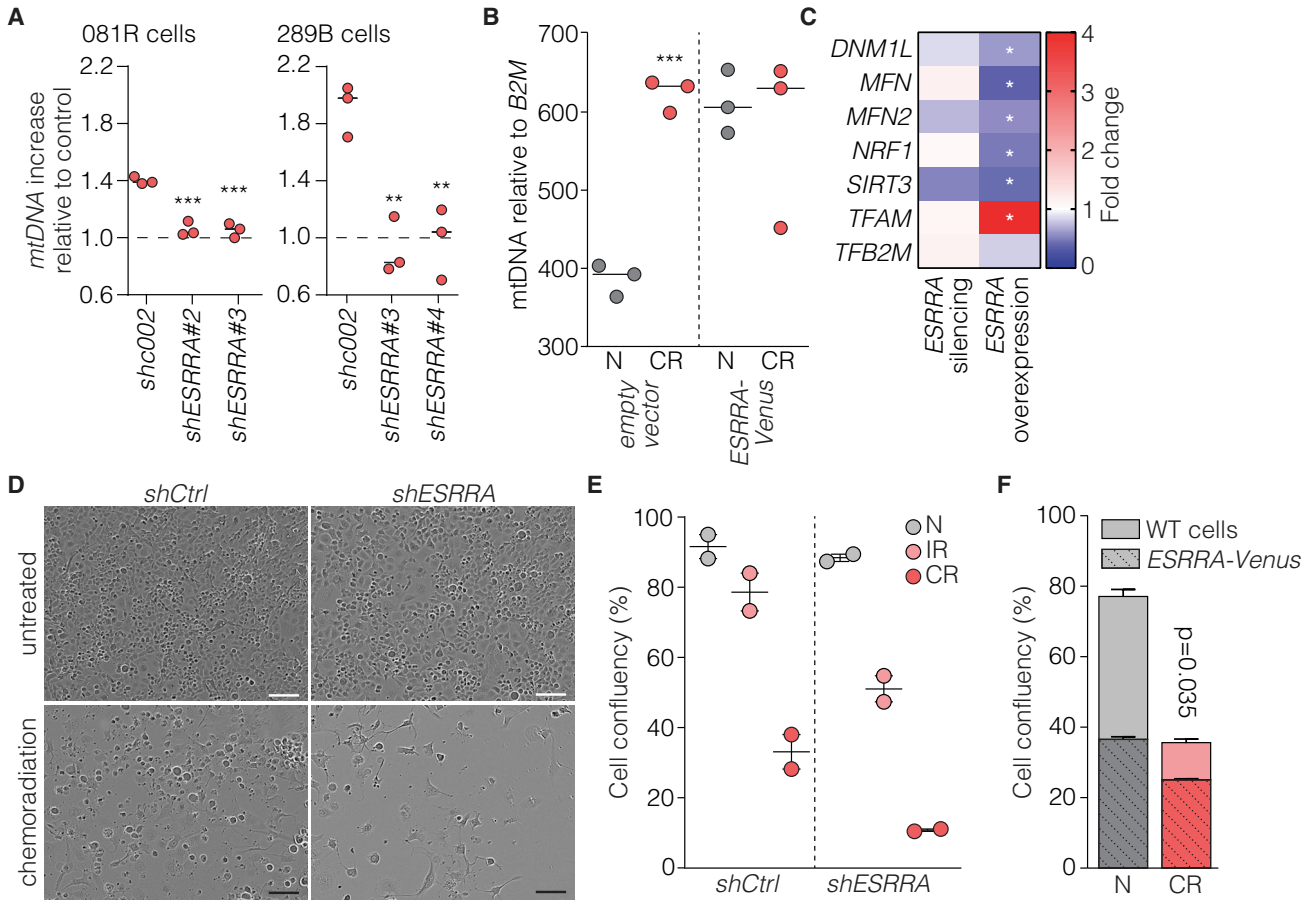


**Figure 4. Genetic perturbation of ESRRA impacts on (chemo)radiation sensitivity**

(A) *ESRRA* knockdown and control cells were exposed to chemoradiation and assessed for mtDNA copy number. Dots indicate technical replicates and fold induction is shown relatively to their untreated control (set to 1). Unpaired t test, $^{**}p < 0.01$, $^{***}p < 0.001$.

(B) Mitochondrial content was determined by qPCR for mtDNA in cells overexpressing ESRRA, and treated as for previous panels. Dots indicate biological replicates. Unpaired t test, $^{***}p < 0.001$.

(C) A selection of known regulators of mitochondrial content and dynamics were measured by qPCR in untreated and 14-day chemoradiated cells. Heatmap indicates fold reduction (blue) or induction (red) of chemoradiated samples compared with control scrambled shRNA and empty vector (both set to 1, not included as a column). Asterisks indicate significance of Mann-Whitney U test $^{*}p < 0.05$.

(D) Phase-contrast microscopy images of untreated and chemoradiated transduced 289B cells with shRNA targeting *ESRRA* or scrambled control, following puromycin selection and validation of knockdown (Figure S4A). Scale bar, 70 μm.

(E) Quantification of confluency as shown in (A), after exposure to indicated conditions. Dots indicate biological duplicates.

(F) EAC cells overexpressing pLeGO-iV2-*ESRRA* or control were cocultured and treated with 14-day chemoradiation or left untreated. Total confluence area of cells, and Venus positive and negative cell area were determined by Incucyte to determine proportional outgrowth. Data are mean percentages of area ± SD of two replicates. p value by one-sided Fisher's exact test.

of ATP synthase to match the other increased electron transport chain components. This effect was counteracted by ESRRAi, suggesting the factors that contribute to membrane potential and mitochondrial biogenesis are connected. In contrast, ESRRAi did not inhibit the increased ROS levels observed after CR (Figure S6C), suggesting that the increase in ROS in response to CR cannot be avoided by preventing mitochondrial biogenesis and that this ROS production is independent of mitochondrial processes regulated by ESRRA.

Having confirmed that ESRRAi inhibits the mitochondrial response to CR, we next treated cells simultaneously with (chemo)radiation and ESRRAi, and measured cell confluence (Figure 5C). As for the silencing approach, the efficacy of both radiation and CR was markedly increased in the presence of ESRRA inhibitor. In accordance, the combination of CR with ESRRAi resulted in dose-dependent apoptosis (Figure S6D). To characterize the synergy landscape across a wide range of radiation doses and ESRRAi concentrations combined, cells were treated with such combinations, cell viability was assessed, and a zero interaction potency model was applied.[27] This revealed high synergy in the 081R cell line (Figure 5D, raw data example of condition indicated by dashed circle shown in inset). Of note, this synergy was less pronounced in the 289B line, which could be explained by the relative sensitivity of this cell line to radiation (see also Figure 5C).

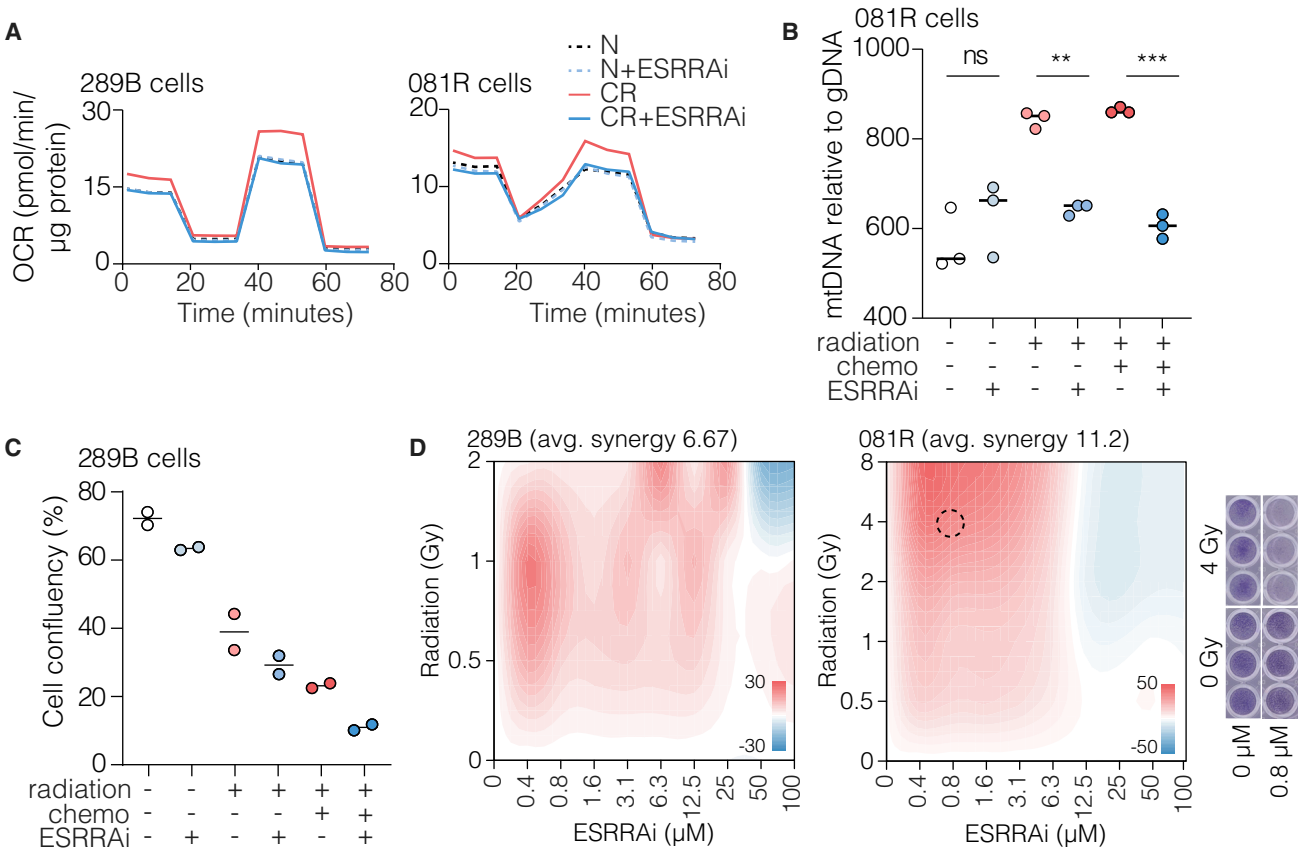


**Figure 5. Pharmacological ESRRA inhibition is synergistic with radiation against EAC cells**

(A) Cells were treated with DMSO, 20 μM ESRRA inhibitor, chemoradiation or both for 14 days and assessed by Seahorse flux analysis. OCR results of mitochondrial stress test of 081R and 289B cells are shown.

(B) Cells were treated with DMSO (N), 20 μM ESRRA inhibitor, radiation, chemoradiation with and without inhibitor and assessed for mtDNA copy number. Unpaired t test **$p < 0.01$, ***$p < 0.001$.

(C) Quantification of confluency following exposure to (chemo)radiation and 20 μM ESRRA inhibitor for 14 days. Dots indicate biological duplicates, no test was applied.

(D) Cells were treated with a range of combined radiation doses and ESRRA inhibitor concentrations. After 72 h, crystal violet stainings were performed and the zero interaction potency (ZIP) model was applied, rendering synergy landscapes of radiation and ESRRA inhibition. Raw data example from condition indicated by dashed circle in landscape plot is shown.

To further ascertain that the effects of ESRRAi hinge on the inhibition of oxidative phosphorylation rather than the perturbance of other processes that also require the presence of mitochondria, we treated cells with oligomycin, an ATP synthase inhibitor. This strongly potentiated the induction of apoptosis in response to CR (Figure S6E). Similar effects were observed using IACS-6274 (an inhibitor of glutamine metabolism[28]), phenformin (a complex I inhibitor), and elesclomol (which shuttles reactive $Cu^{2+}$ to the mitochondria and damages these organelles[29]) (Figure S6F).

## Radiosensitization of preclinical EAC models by ESRRA inhibition

In many patients, the response to neoadjuvant CR followed by surgery is encouraging at first, but most will develop metastatic disease within several years. Emerging data indicate that tumor cells are dependent on oxidative phosphorylation to establish distant micrometastases.[30] To assess whether this is the case in *in vitro* proxies for metastatic outgrowth, we measured both the proliferative and the clonogenic capacity of early-passage patient-derived organoid cultures following treatment (Figure 6A). First, organoids were plated, treated with radiation and ESRRAi, and cell viability was assessed in the days following (Figures 6B and 6C). This revealed that ESRRAi strongly resensitized EAC organoids to radiation. Next, organoids were exposed to radiation and ESRRAi for 2 weeks, and then replated in the absence of either therapy to measure outgrowth capacity (Figure 6D). Single modalities were found to be effective against outgrowth, but the combination of radiation and ESRRAi most effectively thwarted regrowth of organoids suggesting that this combination treatment could also be effective against metastatic disease following regimens with radiation in patients (Figures 6E and 6F).

Next, we aimed to establish efficacy of combined radiation and ESRRA inhibition *in vivo*. NSG mice do not tolerate exposure to radiation, and to allow localized radiation of the tumor we grafted cells in the hindlimb and shielded the body and

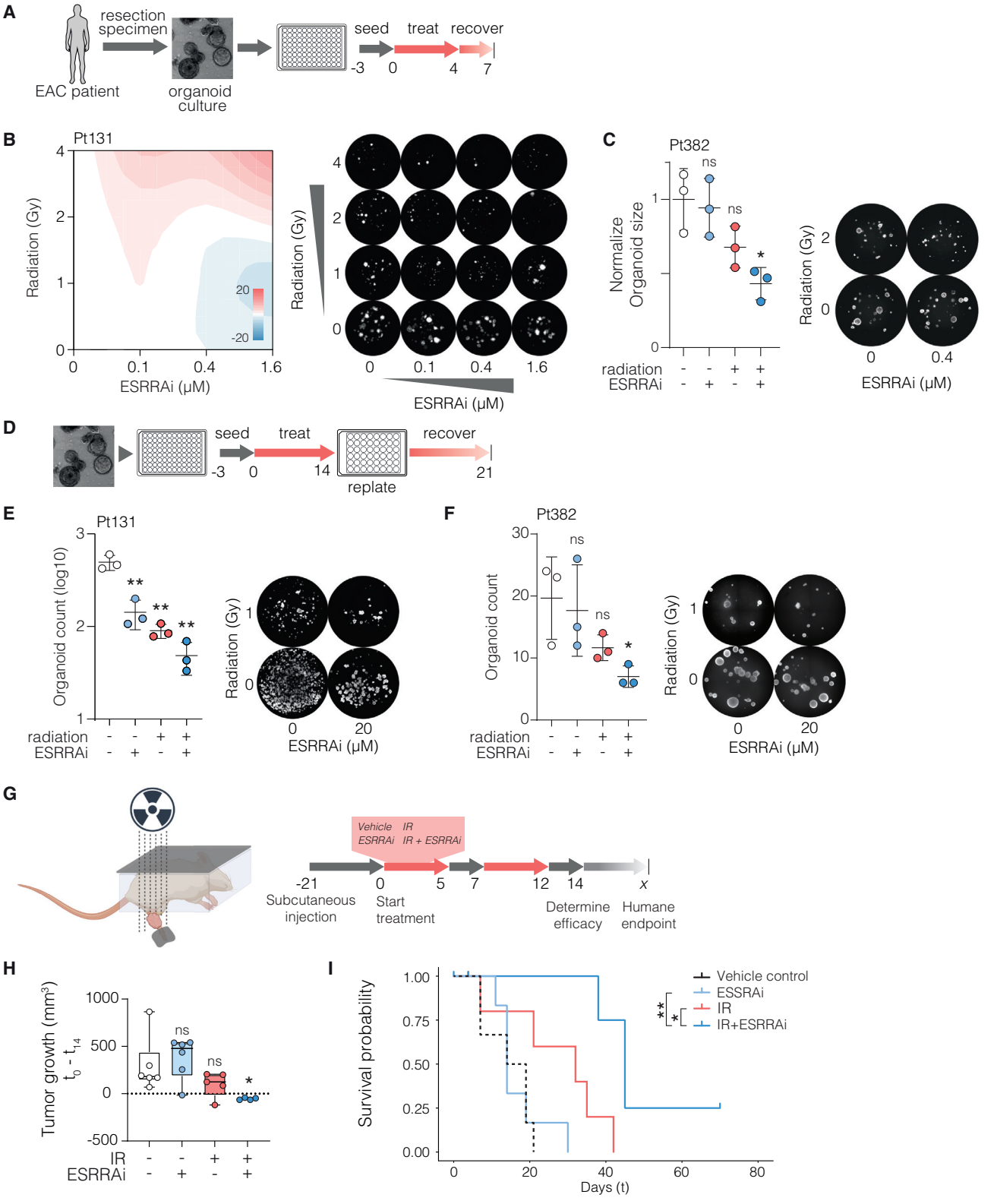


*(legend on next page)*

non-grafted part of the hindlimb with lead when in the radiation setup (Figure 6G). Tumors were grafted and once tumors reached approximately 100 $mm^3$, treatment started (see also Figures S6G and S6H). Directly after treatment, the only group that showed regression was the one that received combined radiation and ESRRAi (Figure 6H, dark blue dots). After 14 days, treatment was stopped, and mice were followed up until the tumors reached a predetermined humane endpoint. Survival was much prolonged in mice that received the combination treatment, offering strong *in vivo* support for the clinical utility of ESRRAi in irradiated esophageal cancers (Figure 6I).

## DISCUSSION

Acquired resistance mechanisms preclude complete efficacy of neoadjuvant CR for the treatment of esophageal cancer. Metabolic rewiring has been observed in numerous cancer contexts, both in unperturbed conditions as well as under treatment. A comprehensive assessment of the cellular responses to CR at the gene expression level in relevant samples and experimental models were lacking thus far in EAC. In the current study, we used matched patient samples before and after neoadjuvant treatment for RNA-seq analysis, and found that under the duress of CR, esophageal cancers upregulate genes associated with oxidative phosphorylation. This observation was functionally validated *in vitro* and revealed that EAC cells elevate oxidative phosphorylation by upregulating mitochondrial content in response to CR-induced ROS production.

Regulation of mitochondrial biogenesis has been attributed to PGC-1$\alpha$,[31,32] which can act together with ESRRA.[21] We observed a crucial dependency on ESRRA to survive in response to CR by upregulating mitochondrial biogenesis, which was not perturbed following knockdown of single *PPARGC1* paralogs. Specifically, we found that forced expression of ESRRA increased resistance against (chemo)radiation, and conversely, its inhibition sensitized radiation-resistant EAC cells. ESRRA inhibition during radiation prevented organoid outgrowth after replating, suggesting the long-term clonogenic potential of EAC cells to be effectively targeted. *In vivo* xenografts were effectively sensitized to radiation by ESRRAi. The profound and rapid changes we observed in mitochondrial content are reminiscent of similar non-metabolic resistance mechanisms previously identified in EAC by our group and others, which suggests these cells have a particularly high degree of plasticity.[33] We propose that the metabolic shifts toward oxidative phosphorylation are the consequence of a widespread reprogramming in response to treatment stress.

We have previously found that CR induces the expression of TGF-$\beta$, and subsequent EMT in EAC cells.[8] EMT itself is known to associate with metabolic reprogramming but typically not with an increase in cellular respiration: For instance, in development, mesenchymal transitions give rise to neural crest cells in which aerobic glycolysis is required for cell migration.[34] Enhanced glycolytic flux has also been observed in cell motility in immune cell migration.[34] In cancer, the mesenchymal transcription factor SNAIL suppresses mitochondrial respiration and consequently induces anaerobic glycolysis in breast cancer.[35] Numerous studies with similar conclusions have been put forward. Recently, however, and in line with our study, chemoresistance has been found to also associate with *increased* mitochondrial respiration in multiple cancer types and regimens applied.[32,36,37] In addition, increased oxidative phosphorylation, rather than the shift to aerobic glycolysis, has been shown to aid the metastatic outgrowth of tumor cells.[30] This suggests that the metabolic reprogramming in chemoresistance is highly context dependent and that increased glycolysis and decreased oxidative phosphorylation are not universal features of mesenchymal transitions and chemoresistance in cancer.

Several potential reasons for the mitochondrial dependency in chemoradiated EAC can be proposed. One is that mitochondria protect cells from excessive ROS.[38] Alternatively, a pool of NAD+ needs to be maintained by the mitochondria, to support PARP activity in response to DNA damage.[39] In addition, the metabolism of glucose through the citric acid cycle converts NAD+ to NADH to support the generation of ATP by oxidative phosphorylation. This is required for both cellular housekeeping as well as increased demands in response to therapeutic stress. We posit that the latter reason (i.e., that the upregulation of oxidative phosphorylation serves to maintain ATP levels)

**Figure 6. ESRRA inhibition radiosensitizes preclinical models for EAC**

(A) Diagram explaining organoid growth assays. Numbers indicate days.

(B) Proliferation by organoid size was determined on patient-131-derived organoids, which were incubated with ESRRAi and/or radiation at indicated concentrations and doses. Shown is synergy landscape rendered for each combination. Representative microscopy images from which synergy landscape was generated are included. Diameter of images is 4.4 mm.

(C) Organoids from patient 382 were treated with indicated doses of radiation and ESRRAi (determined from experiments) shown in (A) and growth expressed as organoid size is shown. Dots indicate biological replicates. Diameter of images is 3.9 mm. Unpaired t test, *$p < 0.05$.

(D) Diagram explaining outgrowth assays.

(E) Clonogenic potential was determined on the same patient-derived organoids as in (A) (patient 131), which were incubated with ESRRAi and/or radiation at indicated concentration/dosages before replating. A quantification of number of counted organoids is shown. Dots indicate biological replicates. Representative images are shown. Diameter of images is 6.8 mm. Unpaired t test, **$p < 0.01$.

(F) As for (C) using patient 382 organoids. Diameter of images is 7.0 mm. Unpaired t test, *$p < 0.05$.

(G) Schematic of setup for radiation treatment of NSG mice, and treatment schedule showing grafting, treatment, and follow-up (units are days). Gray sheets indicate lead shielding. Tumor is grafted on hindlimb ($1 \times 10^5$ cells in 50% Matrigel). At a predetermined start time corresponding to tumor sizes of approximately 100 $mm^3$, treatments commenced. Radiation was 2 × 5 consecutive days, 4 Gy each time to a cumulative dose of 40 Gy. On days of radiation mice also received oral gavages. Solvent was 10% DMSO, 2% Solutol, 70% water and ESRRAi was dosed at 30 mg/kg. Tumor volumes were measured continuously. Once tumors reached 500 $mm^3$, the humane endpoint was reached and mice were culled.

(H) Tumor volumes at start of treatment (t = 0) and end of treatment (t = 14 days) were determined and relative growth in that period was determined. Dots indicate individual mice. Unpaired t test, *$p < 0.05$.

(I) Kaplan-Meier survival analysis of mice. Events are humane endpoints by tumor growth. p value was computed by log rank test.

explains the sensitivity to ESRRA inhibition on a backbone of (chemo)radiation.

We found that highest synergy of ESRRA inhibition was achieved in combination with radiotherapy alone, and that this effect was strongest in those cells that are relatively insensitive to radiation. We therefore envision a clinical application in which ESRRA inhibitors are used to specifically boost the efficacy of radiation in neoadjuvant treatment of EAC and possibly other cancer treatments that rely on radiation. Another advantage of such a regimen comes from the fact that ESRRA inhibition appears to be mostly effective in irradiated cancer cells. Given that irradiation is local, this would provide a focused treatment with potentially lower additional systemic toxicity when ESRRA is included in the CROSS regimen. In addition to the pharmacological prevention of mitochondrial biogenesis, we found that direct inhibition of oxidative phosphorylation by, for instance, oligomycin also synergized with (chemo)radiation. This suggests that other clinically applicable metabolic inhibitors such as Gboxin[40] and IACS-010759[41] could also be considered for investigation.

Of course, the above would require highly accurate patient selection tools. Although we did not identify a predictive signal in pre-treatment biopsies or naive cell cultures, permissive epigenetic landscapes that allow rapid and profound rewiring might exist, and biomarkers that report on this could predict the occurrence of resistance. In addition, it is conceivable that patients are monitored on-treatment for circulating metabolites, or by using functional imaging, to reveal the occurrence of targetable metabolic rewiring.

### Limitations of the study

Several limitations of our study should be acknowledged. Foremost, complete cell kill was not achieved *in vitro* or *in vivo*, nor was full inhibition of regrowth capacity of organoids. While we hypothesize that iterations of combination therapy or alternating regimen of radiation followed by ESRRA inhibitors may well result in complete responses, this remains a topic of future research. Another uncertainty at this moment is whether the observed increase in mitochondria and oxidative phosphorylation in response to CR in patient tissue samples is a consequence of direct instruction of cancer cells, or whether a selection for cells with high oxidative phosphorylation applies. Lineage tracing studies could answer this with certainty.

It should be noted that some ESRRA inhibitors may have nonspecific effects on mitochondrial function that involve, for instance, the PPARGC1 coactivators instead. Given the strict dependence on ESRRA observed in this disease context, the application of such inhibitors should be done with caution.

Despite these limitations, our study provides important insights on how EAC tumors shift their transcriptional program and metabolism to face the challenge of CR. We propose that this knowledge, together with the development of predictive or treatment monitoring tools could be used to improve the efficacy of CR in EAC but possibly other cancer types as well.

## STAR★METHODS

Detailed methods are provided in the online version of this paper and include the following:



## SUPPLEMENTAL INFORMATION

Supplemental information can be found online at https://doi.org/10.1016/j.xcrm.2022.100802.

## ACKNOWLEDGMENTS

We thank the patients for participating. We thank Arlene Oei and Hans Rodermond for their help with the *in vivo* radiation setup. This work was supported by Oncode funding (to J.P.M.) and a KWF Dutch Cancer Society project grant (10992/2017-1) (to M.F.B. and H.W.M.v.L.).

## AUTHOR CONTRIBUTIONS

Design research, A.P.v.d.Z., M.P.G.D., and M.F.B.; data interpretation, analysis, generation, and/or collection, A.P.v.d.Z., M.P.G.D., T.F.J.M., S.B., D.L., A.O., J.P.G.K., T.v.d.E., C.A.S., P.B., J.K., C.W., C.O., G.K.J.H., S.L.M., D.Z., M.I.v.B.H., M.C.H., J.B., H.W.M.v.L., and M.F.B.; supervision of the project, J.P.M., H.W.M.v.L., and M.F.B.; writing the paper, A.P.v.d.Z., M.P.G.D., M.F.B., and H.W.M.v.L.

## DECLARATION OF INTERESTS

M.F.B. has received research funding from Celgene, Frame Therapeutics, and Lead Pharma and has acted as a consultant to Servier. H.W.M.v.L. has a consultant or advisory role with Amphera, AstraZeneca, Beigene, BMS, Daiichy-Sankyo, Dragonfly, Eli Lilly, MSD, Nordic Pharma, and Servier; has received research funding and/or medication supply from Bayer, BMS, Celgene, Janssen, Incyte, Eli Lilly, MSD, Nordic Pharma, Philips, Roche, and

Servier; and has a speaker role with Astellas, Benecke, Daiichy-Sankyo, JAAP, Medtalks, Novartis, and Travel Congress. Management B.V Employment and leadership: Amsterdam UMC, the Netherlands (head of the Department of Medical Oncology) Honorary: ESMO (chair Upper GI faculty).

J.P.M. has acted as a consultant to AbbVie. M.I.v.B.H. served as consultant for Johnson and Johnson, Medtronic, Alesi Surgical, and Mylan and has received unrestricted research funding from Stryker and Olympus. A.O. and J.P.G.K. are employees of Lead Pharma. Lead Pharma owns two patent applications (WO 2021/001453 A1 and WO 2021/074365 A1) claiming the invention of ERRa inverse agonists. The compounds described in these patent applications are not chemically related to the compound described in this manuscript.

Received: December 1, 2021
Revised: June 28, 2022
Accepted: October 12, 2022
Published: November 4, 2022

## SUPPORTING CITATIONS

The following references appear in the Supplemental Information: [53,54,55].

## REFERENCES

1. Bartel, M., Brahmbhatt, B., and Bhurwal, A. (2019). Incidence of gastro-esophageal junction cancer continues to rise: analysis of Surveillance, Epidemiology, and End Results (SEER) database. J. Clin. Oncol. *37*, 40. https://doi.org/10.1200/JCO.2019.37.4.
2. van Hagen, P., Hulshof, M.C.C.M., van Lanschot, J.J.B., Steyerberg, E.W., van Berge Henegouwen, M.I., Wijnhoven, B.P.L., Richel, D.J., Nieuwenhuijzen, G.A.P., Hospers, G.A.P., Bonenkamp, J.J., et al. (2012). Preoperative chemoradiotherapy for esophageal or junctional cancer. N. Engl. J. Med. *366*, 2074–2084. https://doi.org/10.1056/nejmoa1112088.
3. Shapiro, J., van Lanschot, J.J.B., Hulshof, M.C.C.M., van Hagen, P., van Berge Henegouwen, M.I., Wijnhoven, B.P.L., van Laarhoven, H.W.M., Nieuwenhuijzen, G.A.P., Hospers, G.A.P., Bonenkamp, J.J., et al. (2015). Neoadjuvant chemoradiotherapy plus surgery versus surgery alone for oesophageal or junctional cancer (CROSS): long-term results of a randomised controlled trial. Lancet Oncol. *16*, 1090–1098. https://doi.org/10.1016/S1470-2045(15)00040-6.
4. Eyck, B., van Lanschot, J., Hulshof, M., van Berge Henegouwen, M., van Laarhoven, H., Nieuwenhuijzen, G., Hospers, G., Johannes, B., Cuesta, M., Creemers, G.J., et al. (2021). 10-year outcome of a randomized trial comparing neoadjuvant chemoradiotherapy and surgery with surgery alone for esophageal cancer (CROSS trial). Eur. J. Surg. Oncol. *47*, e31. https://doi.org/10.1016/j.ejso.2020.11.225.
5. Oppedijk, V., Van Der Gaast, A., van Lanschot, J.J.B., van Hagen, P., van Os, R., van Rij, C.M., van der Sangen, M.J., Beukema, J.C., Rütten, H., Spruit, P.H., et al. (2014). Patterns of recurrence after surgery alone versus preoperative chemoradiotherapy and surgery in the CROSS trials. J. Clin. Oncol. *32*, 385–391. https://doi.org/10.1200/JCO.2013.51.2186.
6. Ebbing, E.A., Medema, J.P., Damhofer, H., Meijer, S.L., Krishnadath, K.K., van Berge Henegouwen, M.I., Bijlsma, M.F., and van Laarhoven, H.W.M. (2016). ADAM10-mediated release of heregulin confers resistance to trastuzumab by activating HER3. Oncotarget *7*, 10243–10254. https://doi.org/10.18632/oncotarget.7200.
7. Ebbing, E.A., Van Der Zalm, A.P., Steins, A., Creemers, A., Hermsen, S., Rentenaar, R., Klein, M., Waasdorp, C., Hooijer, G.K.J., Meijer, S.L., et al. (2019). Stromal-derived interleukin 6 drives epithelial-to-mesenchymal transition and therapy resistance in esophageal adenocarcinoma. Proc. Natl. Acad. Sci. USA *116*, 2237–2242. https://doi.org/10.1073/pnas.1820459116.
8. Steins, A., Ebbing, E.A., Creemers, A., van der Zalm, A.P., Jibodh, R.A., Waasdorp, C., Meijer, S.L., van Delden, O.M., Krishnadath, K.K., Hulshof, M.C.C.M., et al. (2019). Chemoradiation induces epithelial-to-mesenchymal transition in esophageal adenocarcinoma. Int. J. Cancer *145*, 2792–2803. https://doi.org/10.1002/ijc.32364.
9. Ward, P.S., and Thompson, C.B. (2012). Metabolic reprogramming: a cancer hallmark even warburg did not anticipate. Cancer Cell *21*, 297–308. https://doi.org/10.1016/j.ccr.2012.02.014.
10. Jia, D., Lu, M., Jung, K.H., Park, J.H., Yu, L., Onuchic, J.N., Kaipparettu, B.A., and Levine, H. (2019). Elucidating cancer metabolic plasticity by coupling gene regulation with metabolic pathways. Proc. Natl. Acad. Sci. USA *116*, 3909–3918. https://doi.org/10.1073/pnas.1816391116.
11. Hu, Y., Xu, W., Zeng, H., He, Z., Lu, X., Zuo, D., Qin, G., and Chen, W. (2020). OXPHOS-dependent metabolic reprogramming prompts metastatic potential of breast cancer cells under osteogenic differentiation. Br. J. Cancer *123*, 1644–1655. https://doi.org/10.1038/s41416-020-01040-y.
12. Subramanian, A., Tamayo, P., Mootha, V.K., Mukherjee, S., Ebert, B.L., Gillette, M.A., Paulovich, A., Pomeroy, S.L., Golub, T.R., Lander, E.S., and Mesirov, J.P. (2005). Gene set enrichment analysis: a knowledge-based approach for interpreting genome-wide expression profiles. Proc. Natl. Acad. Sci. USA *102*, 15545–15550. https://doi.org/10.1073/pnas.0506580102.
13. Srinivas, U.S., Tan, B.W.Q., Vellayappan, B.A., and Jeyasekharan, A.D. (2019). ROS and the DNA damage response in cancer. Redox Biol. *25*, 101084. https://doi.org/10.1016/j.redox.2018.101084.
14. Yun, J., and Finkel, T. (2014). Mitohormesis. Cell Metabol. *19*, 757–766. https://doi.org/10.1016/j.cmet.2014.01.011.
15. Cancer Genome Atlas Research Network; Analysis Working Group Asan University; BC Cancer Agency; Brigham and Women's Hospital; Broad Institute; Brown University; Case Western Reserve University; Dana-Farber Cancer Institute; Duke University; Greater Poland Cancer Centre (2017). Integrated genomic characterization of oesophageal carcinoma. Nature *541*, 169–175. https://doi.org/10.1038/nature20805.
16. Peters, C.J., Rees, J.R.E., Hardwick, R.H., Hardwick, J.S., Vowler, S.L., Ong, C.A.J., Zhang, C., Save, V., O'Donovan, M., Rassl, D., et al. (2010). A 4-gene signature predicts survival of patients with resected adenocarcinoma of the esophagus, junction, and gastric cardia. Gastroenterology *139*, 1995–2004.e15. https://doi.org/10.1053/j.gastro.2010.05.080.
17. Krause, L., Nones, K., Loffler, K.A., Nancarrow, D., Oey, H., Tang, Y.H., Wayte, N.J., Patch, A.M., Patel, K., Brosda, S., et al. (2016). Identification of the CIMP-like subtype and aberrant methylation of members of the chromosomal segregation and spindle assembly pathways in esophageal adenocarcinoma. Carcinogenesis *37*, 356–365. https://doi.org/10.1093/carcin/bgw018.
18. Stein, R.A., Chang, C.Y., Kazmin, D.A., Way, J., Schroeder, T., Wergin, M., Dewhirst, M.W., and McDonnell, D.P. (2008). Estrogen-related receptor $\alpha$ is critical for the growth of estrogen receptor-negative breast cancer. Cancer Res. *68*, 8805–8812. https://doi.org/10.1158/0008-5472.CAN-08-1594.
19. Heckler, M.M., Thakor, H., Schafer, C.C., and Riggins, R.B. (2014). ERK/MAPK regulates ERR$\gamma$ expression, transcriptional activity and receptor-mediated tamoxifen resistance in ER+ breast cancer. FEBS J. *281*, 2431–2442. https://doi.org/10.1111/FEBS.12797.
20. Vernier, M., Dufour, C.R., McGuirk, S., Scholtes, C., Li, X., Bourmeau, G., Kuasne, H., Park, M., St-Pierre, J., Audet-Walsh, E., and Giguère, V. (2020). Estrogen-related receptors are targetable ROS sensors. Genes Dev. *34*, 544–559. https://doi.org/10.1101/GAD.330746.119/-/DC1.
21. Singh, B.K., Sinha, R.A., Tripathi, M., Mendoza, A., Ohba, K., Sy, J.A.C., Xie, S.Y., Zhou, J., Ho, J.P., Chang, C.Y., et al. (2018). Thyroid hormone receptor and ERR$\alpha$ coordinately regulate mitochondrial fission, mitophagy, biogenesis, and function. Sci. Signal. *11*, eaam5855. https://doi.org/10.1126/scisignal.aam5855.
22. Virbasius, J.V., and Scarpulla, R.C. (1994). Activation of the human mitochondrial transcriptionfactor A gene by nuclear respiratory factors: a potential regulatory linkbetween nuclear and mitochondrial gene expression in organellebiogenesis. Proc. Natl. Acad. Sci. USA *91*, 1309–1313. https://doi.org/10.1073/PNAS.91.4.1309.

23. Huss, J.M., Kopp, R.P., and Kelly, D.P. (2002). Peroxisome proliferator-activated receptor coactivator-1α (PGC-1α) coactivates the cardiac-enriched nuclear receptors estrogen-related receptor-α and -γ: identification of novel leucine-rich interaction motif within PGC-1α. J. Biol. Chem. *277*, 40265–40274. https://doi.org/10.1074/JBC.M206324200.

24. Schreiber, S.N., Knutti, D., Brogli, K., Uhlmann, T., and Kralli, A. (2003). The transcriptional coactivator PGC-1 regulates the expression and activity of the orphan nuclear receptor estrogen-related receptor α (ERRα). J. Biol. Chem. *278*, 9013–9018. https://doi.org/10.1074/JBC.M212923200.

25. Sonoda, J., Laganière, J., Mehl, I.R., Barish, G.D., Chong, L.W., Li, X., Scheffler, I.E., Mock, D.C., Bataille, A.R., Robert, F., et al. (2007). Nuclear receptor ERRα and coactivator PGC-1β are effectors of IFN-γ-induced host defense. Genes Dev. *21*, 1909–1920. https://doi.org/10.1101/GAD.1553007.

26. Patch, R.J., Searle, L.L., Kim, A.J., De, D., Zhu, X., Askari, H.B., O'Neill, J.C., Abad, M.C., Rentzeperis, D., Liu, J., et al. (2011). Identification of diaryl ether-based ligands for estrogen-related receptor α as potential antidiabetic agents. J. Med. Chem. *54*, 788–808. https://doi.org/10.1021/jm101063h.

27. Yadav, B., Wennerberg, K., Aittokallio, T., and Tang, J. (2015). Searching for drug synergy in complex dose-response landscapes using an interaction potency model. Comput. Struct. Biotechnol. J. *13*, 504–513. https://doi.org/10.1016/j.csbj.2015.09.001.

28. Yap, T.A., Dumbrava, E.E., Rodon Ahnert, J., Hong, D.S., Pant, S., Karp, D.D., Piha-Paul, S.A.A., Subbiah, V., Tsimberidou, A.M., Fu, S., et al. (2021). First-in-human biomarker-driven phase I trial of the potent and selective glutaminase-1 (GLS1) inhibitor IACS-6274 (IPN60090) in patients (pts) with molecularly selected advanced solid tumors. J. Clin. Orthod. *39*, 3001. https://doi.org/10.1200/JCO. 39.15_suppl.3001.

29. Tsvetkov, P., Coy, S., Petrova, B., Dreishpoon, M., Verma, A., Abdusamad, M., Rossen, J., Joesch-Cohen, L., Humeidi, R., Spangler, R.D., et al. (2022). Copper induces cell death by targeting lipoylated TCA cycle proteins. Science *375*, 1254–1261. https://doi.org/10.1126/science.abf0529.

30. Davis, R.T., Blake, K., Ma, D., Gabra, M.B.I., Hernandez, G.A., Phung, A.T., Yang, Y., Maurer, D., Lefebvre, A.E.Y.T., Alshetaiwi, H., et al. (2020). Transcriptional diversity and bioenergetic shift in human breast cancer metastasis revealed by single-cell RNA sequencing. Nat. Cell Biol. *22*, 310–320. https://doi.org/10.1038/s41556-020-0477-0.

31. Spiegelman, B.M., and Heinrich, R. (2004). Biological control through regulated transcriptional coactivators. Cell *119*, 157–167. https://doi.org/10.1016/j.cell.2004.09.037.

32. Vellinga, T.T., Borovski, T., de Boer, V.C.J., Fatrai, S., van Schelven, S., Trumpi, K., Verheem, A., Snoeren, N., Emmink, B.L., Koster, J., et al. (2015). SIRT1/PGC1a-Dependent increase in oxidative phosphorylation supports chemotherapy resistance of colon cancer. Clin. Cancer Res. *21*, 2870–2879. https://doi.org/10.1158/1078-0432.CCR-14-2290.

33. Steins, A., Ebbing, E.A., Creemers, A., van der Zalm, A.P., Jibodh, R.A., Waasdorp, C., Meijer, S.L., van Delden, O.M., Krishnadath, K.K., Hulshof, M.C.C.M., et al. (2019). Chemoradiation induces epithelial-to-mesenchymal transition in esophageal adenocarcinoma. Int. J. Cancer *145*, 2792–2803. https://doi.org/10.1002/ijc.32364.

34. Bhattacharya, D., Azambuja, A.P., and Simoes-Costa, M. (2020). Metabolic reprogramming promotes neural crest migration via Yap/Tead signaling. Dev. Cell *53*, 199–211.e6. https://doi.org/10.1016/j.devcel.2020.03.005.Metabolic.

35. Lee, S.Y., Jeon, H.M., Ju, M.K., Kim, C.H., Yoon, G., Han, S.I., Park, H.G., and Kang, H.S. (2012). Wnt/snail signaling regulates cytochrome c oxidase and glucose metabolism. Cancer Res. *72*, 3607–3617. https://doi.org/10.1158/0008-5472.CAN-12-0006.

36. Lee, K.M., Giltnane, J.M., Balko, J.M., Schwarz, L.J., Guerrero-Zotano, A.L., Hutchinson, K.E., Nixon, M.J., Estrada, M.V., Sánchez, V., Sanders, M.E., and Lee, T. (2018). MYC and MCL1 cooperatively promote chemotherapy- resistant breast cancer stem cells via regulation of mitochondrial oxidative phosphorylation. Cell Metabol. *26*, 633–647. https://doi.org/10.1016/j.cmet.2017.09.009.

37. Farge, T., Saland, E., de Toni, F., Aroua, N., Hosseini, M., Perry, R., Bosc, C., Sugita, M., Stuani, L., Fraisse, M., et al. (2017). Chemotherapy resistant human acute myeloid leukemia cells are not enriched for leukemic stem cells but require oxidative metabolism. Cancer Discov. *7*, 716–735. https://doi.org/10.1158/2159-8290.CD-16-0441.

38. Starkov, A.A. (2008). The role of mitochondria in reactive oxygen species metabolism and signaling. Ann. N. Y. Acad. Sci. *1147*, 37–52. https://doi.org/10.1196/annals.1427.015.

39. Lahiguera, Á., Hyroššová, P., Figueras, A., Garzón, D., Moreno, R., Soto-Cerrato, V., McNeish, I., Serra, V., Lazaro, C., Barretina, P., et al. (2020). Tumors defective in homologous recombination rely on oxidative metabolism: relevance to treatments with PARP inhibitors. EMBO Mol. Med. *12*, e11217–e11223. https://doi.org/10.15252/emmm.201911217.

40. Shi, Y., Lim, S.K., Liang, Q., Iyer, S.V., Wang, H.Y., Wang, Z., Xie, X., Sun, D., Chen, Y.J., Tabar, V., et al. (2019). Gboxin is an oxidative phosphorylation inhibitor that targets glioblastoma. Nature *567*, 341–346. https://doi.org/10.1038/s41586-019-0993-x.

41. Molina, J.R., Sun, Y., Protopopova, M., Gera, S., Bandi, M., Bristow, C., McAfoos, T., Morlacchi, P., Ackroyd, J., Agip, A.N.A., et al. (2018). An inhibitor of oxidative phosphorylation exploits cancer vulnerability. Nat. Med. *24*, 1036–1046. https://doi.org/10.1038/s41591-018-0052-4.

42. Koster, J., R2: genomics analysis and visualization platform. https://hgserver1.amc.nl/cgi-bin/r2/main.cgi?open_page=login.

43. Dull, T., Zufferey, R., Kelly, M., Mandel, R.J., Nguyen, M., Trono, D., and Naldini, L. (1998). A third-generation lentivirus vector with a conditional packaging system. J. Virol. *72*, 8463–8471. https://doi.org/10.1128/JVI.72.11.8463-8471.1998.

44. Sato, T., Stange, D.E., Ferrante, M., Vries, R.G.J., Van Es, J.H., Van den Brink, S., Van Houdt, W.J., Pronk, A., Van Gorp, J., Siersema, P.D., and Clevers, H. (2011). Long-term expansion of epithelial organoids from human colon, adenoma, adenocarcinoma, and Barrett's epithelium. Gastroenterology *141*, 1762–1772. https://doi.org/10.1053/j.gastro.2011.07.050.

45. Murtha, M., Tokcaer-Keskin, Z., Tang, Z., Strino, F., Chen, X., Wang, Y., Xi, X., Basilico, C., Brown, S., Bonneau, R., et al. (2014). FIREWACh: high-throughput functional detection of transcriptional regulatory modules in mammalian cells. Nat. Methods *11*, 559–565. https://doi.org/10.1038/nmeth.2885.

46. Weber, K., Bartsch, U., Stocking, C., and Fehse, B. (2008). A multicolor panel of novel lentiviral "gene ontology" (LeGO) vectors for functional gene analysis. Mol. Ther. *16*, 698–706. https://doi.org/10.1038/mt.2008.6.

47. Eide, P.W., Bruun, J., Lothe, R.A., and Sveen, A. (2017). CMScaller: an R package for consensus molecular subtyping of colorectal cancer pre-clinical models. Sci. Rep. *7*, 16618. https://doi.org/10.1038/s41598-017-16747-x.

48. Bioconductor fgsea. http://bioconductor.org/packages/fgsea/.

49. Damhofer, H., Ebbing, E.A., Steins, A., Welling, L., Tol, J.A., Krishnadath, K.K., van Leusden, T., van de Vijver, M.J., Besselink, M.G., Busch, O.R., et al. (2015). Establishment of patient-derived xenograft models and cell lines for malignancies of the upper gastrointestinal tract. J. Transl. Med. *13*, 115. https://doi.org/10.1186/s12967-015-0469-1.

50. van den Ende, T., de Clercq, N.C., van Berge Henegouwen, M.I., Gisbertz, S.S., Geijsen, E.D., Verhoeven, R.H.A., Meijer, S.L., Schokker, S., Dings, M.P.G., Bergman, J.J.G.H.M., et al. (2021). Neoadjuvant chemoradiotherapy combined with atezolizumab for resectable esophageal adenocarcinoma: a single arm phase II feasibility trial (PERFECT). Clin. Cancer Res. *27*, 3351–3359. https://doi.org/10.1158/1078-0432.CCR-20-4443.

51. Li, X., Francies, H.E., Secrier, M., Perner, J., Miremadi, A., Galeano-Dalmau, N., Barendt, W.J., Letchford, L., Leyden, G.M., Goffin, E.K., et al. (2018). Organoid cultures recapitulate esophageal adenocarcinoma heterogeneity providing a model for clonality studies and precision

therapeutics. Nat. Commun. *9*, 2983–3013. https://doi.org/10.1038/s41467-018-05190-9.

52. Liberzon, A., Birger, C., Thorvaldsdóttir, H., Ghandi, M., Mesirov, J.P., and Tamayo, P. (2015). The Molecular Signatures Database (MSigDB) hallmark gene set collection. Cell Syst. *1*, 417–425. https://doi.org/10.1016/j.cels.2015.12.004.

53. Yoshihara, K., Shahmoradgoli, M., Martínez, E., Vegesna, R., Kim, H., Torres-Garcia, W., Treviño, V., Shen, H., Laird, P.W., Levine, D.A., et al. (2013). Inferring tumour purity and stromal and immune cell admixture from expression data. Nat. Commun. *4*, 2612. https://doi.org/10.1038/ncomms3612.

54. Mandard, A.M., Dalibard, F., Mandard, J.C., Marnay, J., Henry-Amar, M., Petiot, J.F., Roussel, A., Jacob, J.H., Segol, P., Samama, G., and Ollivier, J.M. (1994). Pathologic assessment of tumor regression after preoperative chemoradiotherapy of esophageal carcinoma. Clinicopathologic correlations *73*, 2680–2686. https://doi.org/10.1002/1097-0142(19940601)73:11.

55. Boland, M.L., Chourasia, A.H., and Macleod, K.F. (2013). Mitochondrial dysfunction in cancer. Front. Oncol. *3*, 292–328. https://doi.org/10.3389/fonc.2013.00292.

## STAR★METHODS

### KEY RESOURCES TABLE

| REAGENT or RESOURCE | SOURCE | IDENTIFIER |
|---|---|---|
| Antibodies | | |
| anti-COX4 | Cell Signaling | 4850; RRID:AB_2085424 |
| anti-Vinculin | Cell Signaling | 13901-S; RRID:AB_2728768 |
| anti-ESRRA | Merck | HPA053785; RRID:AB_2682260 |
| anti-ESRRA | Abcam | Ab76228; RRID:AB_1523580 |
| anti-beta-I tubulin | Sigma | T7816; RRID:AB_261770 |
| Alexa 488 anti-rabbit IgG (H+L) | Invitrogen | A11008; RRID:AB_143165 |
| Alexa568 anti-mouse IgG1 | Invitrogen | A21124; RRID:AB_2535766 |
| HRP anti-mouse IgG (H+L) | Molecular Probes | 1031-05; RRID:AB_2794307 |
| Bacterial and virus strains | | |
| TOP10 competent *E. coli* DH5-alpha | C2987H | NEB |
| 3rd generation lentiviral system | AddGene/Trono lab[43] | N/A |
| Biological samples | | |
| Fresh frozen pre- and post-nCRT samples | AMC | N/A |
| FFPE embedded pre- and post-nCRT samples | AMC | N/A |
| Chemicals, peptides, and recombinant proteins | | |
| Matrigel | Corning | 356213 |
| Organoid supplements | See ref.[44] | N/A |
| Advanced DMEM F/12 | Gibco | 12634010 |
| Gentamycin | Lonza | 17-519Z |
| B27 Supplement | Invitrogen | 17504-044 |
| N-acetylcysteine (NAC) | Medkoo Biosciences | 317102 |
| Gastrin | Tocris | 3006 |
| EGF | Peprotech | 100-15 |
| WNT3A conditioned medium | Prepared in-house | See ref.[44] |
| RSPO-1 conditioned medium | Prepared in-house | See ref.[44] |
| Noggin-conditioned medium | Prepared in-house | See ref.[44] |
| FGF-10 | Peprotech | 100-26 |
| Nicotinamide | Sigma-Aldrich | N-7004 |
| A-83-01 ALK5 inhibitor | Tocris | 803 |
| ROCK inhibitor | Sigma-Aldrich | Y0503 |
| Carboplatin | AMC pharmacy | N/A |
| Paclitaxel | AMC pharmacy | N/A |
| Lipofectamine | Invitrogen | 11668-019 |
| N-acetylcysteine (NAC) | Sigma-Aldrich | A9165-25g |
| MitoQ | Medkoo Biosciences | 317102 |
| Oligomycin | Sigma-Aldrich | O4876 |
| IACS-6274 | MedChemExpress | HY-112037 |
| Phenformin | MedChemExpress | HY-16397A |
| Elesclomol | MedChemExpress | HY-12040 |
| MitoTracker Green | ThermoFisher | M46750 |
| MitoTracker Deep Red FM | ThermoFisher | M22426 |
| DCFDA | Sigma-Aldrich | D6883-50MG |
| Hoechst | ThermoFisher | 62249 |
| ESSRA inhibitor | Lead Pharma | LP 0821[26] |

(*Continued on next page*)

*Continued*

| REAGENT or RESOURCE | SOURCE | IDENTIFIER |
|---|---|---|
| ESSRA inhibitor | Lead Pharma | LP 0811 |
| JC-1 | ThermoFisher | T3168 |
| **Critical commercial assays** | | |
| AllPrep DNA/RNA/miRNA Universal Kit | Qiagen | 80224 |
| Total RNA library prep RiboErase | Roche | KR1351 |
| QuickExtract | Lucigen | QE09050 |
| Cut&Run Assay kit | Cell Signaling | 86652 |
| Dual-Luciferase® Reporter Assay System | Promega | E1910 |
| Pierce™ BCA Protein Assay Kit | Thermo Scientific | 23225 |
| **Deposited data** | | |
| RNA-Seq data pre- and post-treatment | GEO | GSE184654 |
| **Experimental models: Cell lines** | | |
| HEK293T cell line | ATCC | CRL-3216; RRID:CVCL_0063 |
| OE19 cell line | DSMZ | ACC 700; RRID:CVCL_1622 |
| OE33 cell line | DSMZ | ACC 706; RRID:CVCL_0471 |
| Flo-1 cell line | DSMZ | ACC 698; RRID:CVCL_2045 |
| 037M primary line | AMC | AMC_EAC_037M |
| 081R primary line | AMC | AMC_EAC_081R |
| 007B primary line | AMC | AMC_EAC_007B |
| 289B primary line | AMC | AMC_EAC_289B |
| 058M primary line | AMC | AMC_EAC_058M |
| 031M primary line | AMC | AMC_EAC_031M |
| Pt131 organoid culture | AMC | PERFECT_131 |
| Pt382 organoid culture | AMC | AMC_EAC_382 |
| **Experimental models: Organisms/strains** | | |
| NOD.Cg-*Prkdc*$^{scid}$*Il2rg*$^{tm1Wjl}$/SzJ (NSG) | Own breeding | N/A |
| **Oligonucleotides** | | |
| Fw *mTL1* cacccaagaacagggtttgt (mtDNA) | Sigma-Aldrich | N/A |
| Rv *mTL1* tggccatgggtatgttgtta (mtDNA) | Sigma-Aldrich | N/A |
| Fw *B2M* tgctgtctccatgtttgatgtatct (gDNA) | Sigma-Aldrich | N/A |
| Rv *B2M* tctctgctccccacctctaagt (gDNA) | Sigma-Aldrich | N/A |
| Fw *B2M* gtctttcagcaaggactggtc (cDNA) | Sigma-Aldrich | N/A |
| Rv *B2M* cttcaaacctccatgatgc (cDNA) | Sigma-Aldrich | N/A |
| Fw *RPS18* agttccagcatattttgcgag | Sigma-Aldrich | N/A |
| Rv *RPS18* ctcttggtgaggtcaatgtc | Sigma-Aldrich | N/A |
| Fw *ESRRA* ggctggagcgagaggagtatg | Sigma-Aldrich | N/A |
| Rv *ESRRA* ggaggagcggtagcgtgag | Sigma-Aldrich | N/A |
| Fw *DNML1* gatgccatagttgaagtggtgac | Sigma-Aldrich | N/A |
| Rv *DNML1* ccacaagcatcagcaaagtctgg | Sigma-Aldrich | N/A |
| Fw *MFN* ggtgaatgagcggctttccaag | Sigma-Aldrich | N/A |
| Rv *MFN* tcctccaccaagaaatgcaggc | Sigma-Aldrich | N/A |
| Fw *MFN2* attgcagaggcggttcgactca | Sigma-Aldrich | N/A |
| Rv *MFN2* ttcagtcggtcttgccgctctt | Sigma-Aldrich | N/A |
| Fw *NRF1* ggcaacagtagccacattggct | Sigma-Aldrich | N/A |
| Rv *NRF1* gtcgtctggatggtcatctcac | Sigma-Aldrich | N/A |
| Fw *SIRT3* ccctggaaactacaagcccaac | Sigma-Aldrich | N/A |
| Rv *SIRT3* gcagaggcaaaggttccatgag | Sigma-Aldrich | N/A |
| Fw *TFAM* gtggttttcatctgtcttggcaag | Sigma-Aldrich | N/A |

(*Continued on next page*)

*Continued*

| REAGENT or RESOURCE | SOURCE | IDENTIFIER |
|---|---|---|
| Rv *TFAM* ttccctccaacgctgggcaatt | Sigma-Aldrich | N/A |
| Fw *TFB2M* gggaaaaccaagtagacctccac | Sigma-Aldrich | N/A |
| Rv *TFB2M* tttcgagcgcaaccactttggc | Sigma-Aldrich | N/A |
| Fw *PPARGC1A* ccaaaggatgcgctctcgttca | Sigma-Aldrich | N/A |
| Rv *PPARGC1A* cggtgtctgtagtggcttgact | Sigma-Aldrich | N/A |
| Fw *PPARGC1B* tgagcagaccttgacagtggag | Sigma-Aldrich | N/A |
| Rv *PPARGC1B* gactatgcttgatgtctggtttga | Sigma-Aldrich | N/A |
| Fw *GLUT1* gtggagactaagccctgtcg | Sigma-Aldrich | N/A |
| Rv *GLUT1* aggggcaaatcctaatggag | Sigma-Aldrich | N/A |
| Fw *HK2* agagaggaccccactggac | Sigma-Aldrich | N/A |
| Rv *HK2* ccaaggtgaagcaaccgtat | Sigma-Aldrich | N/A |
| Fw *GAPDH* aatcccatcaccatcttcca | Sigma-Aldrich | N/A |
| Rv *GAPDH* tggactccacgacgtactca | Sigma-Aldrich | N/A |
| Fw *PGK1* agagccagttgctgtagaactcaa | Sigma-Aldrich | N/A |
| Rv *PGK1* ctgggcctacacagtccttca | Sigma-Aldrich | N/A |
| Fw *ENO1* cacagtgaccaacccaaaga | Sigma-Aldrich | N/A |
| Rv *ENO1* aacgatgagacaccatgacg | Sigma-Aldrich | N/A |
| Fw *LDHA* gacctacgtggcttggaaga | Sigma-Aldrich | N/A |
| Rv *LDHA* ttcagagagacaccagcaaca | Sigma-Aldrich | N/A |
| Fw *PDK* ggttgggaaccactctttca | Sigma-Aldrich | N/A |
| Rv *PDK* gctttggttacgtggcattt | Sigma-Aldrich | N/A |
| Fw *IDH2* ctcagcctgggctccacggttg | Sigma-Aldrich | N/A |
| Rv *IDH2* ggtctctgagggtttgacacatc | Sigma-Aldrich | N/A |
| Fw *IDH3B* cactgcttgctcacgcctgtttc | Sigma-Aldrich | N/A |
| Rv *IDH3B* cactgcttgctcacgcctgtttc | Sigma-Aldrich | N/A |
| Fw *SDHA* ctcggtccttagtagatagtccgcgtc | Sigma-Aldrich | N/A |
| Rv *SDHA* caggacaacccgcacagagg | Sigma-Aldrich | N/A |
| Fw negCTRL acatgttgggactgttgcca | Sigma-Aldrich | N/A |
| Rv negCTRL gttccacctcagactgcaca | Sigma-Aldrich | N/A |
| **Recombinant DNA** | | |
| pLKO.1 sh*ESRRA* | Mission TRC library | TRCN0000022180 |
| pLKO.1 sh*ESRRA* | Mission TRC library | TRCN0000022181 |
| pLKO.1 sh*ESRRA* | Mission TRC library | TRCN0000022182 |
| pLKO.1 sh*PPARGC1A* | Mission TRC library | TRCN0000001165 |
| pLKO.1 sh*PPARGC1A* | Mission TRC library | TRCN0000001166 |
| pLKO.1 sh*PPARGC1A* | Mission TRC library | TRCN0000001168 |
| pLKO.1 sh*PPARGC1B* | Mission TRC library | TRCN0000008597 |
| pLKO.1 sh*PPARGC1B* | Mission TRC library | TRCN0000008599 |
| pLKO.1 sh*PPARGC1B* | Mission TRC library | TRCN0000008601 |
| pLKO.1 shc002 | Mission TRC library | N/A |
| pGL3*ESRRA* luciferase reporter | AddGene and ref.[19] | 37851 |
| FpG5 GFP reporter | AddGene and ref.[45] | 69443 |
| pLEGO-V2 | AddGene and ref.[46] | 27340 |
| pLEGO-iV2-*PPARGC1A* | GenScript | PPARGC1A_OHu27412C_pLEGO-iV2 |
| pLEGO-iV2-*ESRRA* | GenScript | ESRRA_OHu20547C_pLEGO-iV2 |
| pMD2.G | AddGene/Trono lab[43] | 12259 |
| pMDLg/pRRE | AddGene/Trono lab | 12251 |
| pRSV-Rev | AddGene/Trono lab | 12253 |

(*Continued on next page*)

*Continued*

| REAGENT or RESOURCE | SOURCE | IDENTIFIER |
|---|---|---|
| Software and algorithms | | |
| ImageJ software | NIH | Version 1.5050i |
| Graphpad Prism | GraphPad Software | Version 9.3.1 |
| IncuCyte™ base analysis software | Sartorius | Incucyte2021C |
| R2 bioinformatics platform | R2.amc.nl | Accessed 2021 |
| CMScaller | See ref.[47] | N/A |
| fGSEA | See ref.[48] | N/A |
| Synergy score calculator | See ref.[27] | N/A |
| Other | | |
| Seahorse XF96 Extracellular Flux Analyzer | Agilent | Seahorse XFe96 Analyzer |
| Confocal microscope | Leica | SP8-X |
| Transmission electron microscope | ThermoFisher | FEI Tecnai T12 |
| LC480 II Lightcycler | Roche | 05015243001 |
| CytoFLEX-S FACS | BeckmanCoulter | B75442 |
| FACS cell sorter | Sony | SH800 |
| Spectral FACS | Sony | SP6800 |
| IncuCyte™ S3 | Sartorius | 4647 |
| EVOS FL Auto | ThermoFisher | AMAFD1000 |
| ImageXpress Pico | Molecular Devices | ImageXpress Pico |
| Plate spectrophotometer | BioTek Instruments | Biotek HT |
| Sonicator | Qsonica | Q800R |
| Radiation source (animals) | XStrahl | RS320 |
| Radiation source (cells) | Precision Xray | CellRad |

## RESOURCE AVAILABILITY

### Lead contact

Further information and requests for resources and reagents should be directed to and will be fulfilled by the lead contact, Maarten Bijlsma (m.f.bijlsma@amsterdamumc.nl).

### Materials availability

All unique/stable reagents generated in this study are available from the lead contact with a completed materials transfer agreement.

### Data and code availability

- RNA-Seq data have been deposited at Gene Expression Omnibus (GEO) under accession number GSE184654 and is publicly available as of the date of publication.
- All the R scripts used in this study are available upon request and without restriction to the lead contact (m.f.bijlsma@amsterdamumc.nl).
- Any additional information required to reanalyze the data reported in this work paper is available from the lead contact upon request.

## EXPERIMENTAL MODEL AND SUBJECT DETAILS

### Patient samples

All patient material, primary cell lines, and clinical data were collected with consent under ethical approval (METC 2013_241). Organoid Pt131 was under approval METC 2017_0120. Organoid Pt382 was under approval METC 2013_241. Primary cell lines were obtained and established in agreement with pertinent legislation, Declaration of Helsinki, and patient's informed consent.[49] Baseline characteristics are stated in Table S1 (RNA-Seq discovery cohort), Table S2 (FFPE validation cohort, IDs for both cohorts and overlap listed in Table S3), Table S4 (patient-derived cell lines).

### Cell culture

Flo1, OE19 and OE33 cells (DSMZ, Germany) were maintained in RPMI, and HEK293T, 058M, 081R and 289B were in DMEM, both with 4.5 g/L glucose, 8% fetal bovine serum, L-glutamine (2 mmol/L), penicillin (100 units/mL), and streptomycin (500 μg/mL; all from Lonza, Basel, Switzerland). 031M, 037M and 007B were maintained in Advanced DMEM/F12 (Gibco; 3.1 g/L glucose) with 1:100 N2 (Invitrogen), 2 mM L-glutamine (Sigma-Aldrich), 5 mM HEPES (Life Technologies), 0.15% D-glucose (Sigma-Aldrich), 100 μM β-mercaptoethanol (Sigma-Aldrich), 10 μg/mL insulin (Sigma-Aldrich), 2 μg/mL heparin (Sigma-Aldrich), and 1:1000 trace elements B and C (Fisher Scientific, Waltham, MA). All cell lines were tested for mycoplasma monthly, and STR profiled (Table S5). Medium was refreshed regularly (2 times per week) to avoid nutrients becoming limiting. Cultures were normoxic at all times.

### EAC organoids

The organoid culture Pt131 was established from an EAC resection specimen from a male patient, 69 years of age. Prior to surgery, the patient received neoadjuvant chemotherapy according to the CROSS regimen, in combination with atezolizumab in the PERFECT trial (NCT03087864[50]). Organoid culture Pt382 was established from an EAC resection specimen from a male patient, 64 years of age. Patient received standard of care neoadjuvant chemotherapy according to CROSS. Organoids were established using published methods.[51] Organoids were grown in a Matrigel cushion, using the following medium: Advanced DMEM/F12 (Invitrogen, Waltham, MA) with Glutamax (2 mmol/L), penicillin (100 units/mL), and streptomycin (500 μg/mL; all from Lonza, Basel, Switzerland), HEPES (15630-056, Thermo Fisher, Waltham, MA), 2% B27 (Invitrogen, Waltham, MA), 1 mM N-acetylcysteine (Sigma, St Louis, MO), 10 nM Gastrin (Sigma, St Louis, MO), 50 ng/mL EGF (Peprotech, Rocky Hill, US), 50% Wnt3a conditioned medium and 10% RSPO1-conditioned media (both made in-house), 10% 100 ng/mL Noggin (Peprotech, Rocky Hill, US), 10 mM Nicotinamide (Sigma, St Louis, MO) and A83-01 (Tocris, Abingdon, UK). Next generation sequencing (Ion AmpliSeq NGS, Thermo Fisher, Waltham, MA) with a custom-made gastroesophageal cancer panel revealed mutations in *CDKN2A*, *PCLO*, and *TP53*, confirming the Pt131 organoid to be of tumor origin.

### Animal studies

Animal work procedures were approved by the animal experimental committee (Instantie voor Dierenwelzijn) of the institute according to Dutch law and performed in accordance with ethical and procedural guidelines established by the Amsterdam UMC, location AMC and Dutch legislation. Ethical approval number is AVD1180020171672. NOD.Cg-Prkdc$^{scid}$ Il2rg$^{tm1Wjl}$/Szj (NSG) mice were bred in-house. Animals were kept at room temperature in a DM2/ML2 animal facility, and were specific pathogen-free. From 10 weeks of age, mice were included in the experiment, and subcutaneously injected in the right hind limb. $1 \times 10^5$ cells were injected in a volume of 100μL with 50% medium and 50% Matrigel. At a tumor size of approximately 100 mm,$^3$ mice were randomized to treatment groups. Males and females were equally distributed. All experiments ended for individual mice either when the total tumor volume exceeded 500 mm,$^3$ when the tumor showed ulceration, in case of serious clinical illness, when the tumor growth blocked the movement of the mouse, or when tumor growth assessment had been completed.

## METHOD DETAILS

### Chemoradiation protocol

Carboplatin and paclitaxel were purchased from the pharmacy of the Academic Medical Center. All cell lines were challenged with the following 2-week regimen as described before[8]: Day 1, one single dose of carboplatin at 2 μM and paclitaxel at 0.05 nM combined with 1 Gy radiation; day 2–5, 1 Gy radiation per day; day 6–7, no therapy. This cycle was repeated on day 8 until day 14. 031M and 007B cells received the same schedule using carboplatin at 20 μM and paclitaxel at 0.5 nM.

### Electron microscopy

Cells were treated with chemoradiation (14 days) or control. All samples were fixed in 0.1M PHEM buffer, 2% paraformaldehyde, and 0.2% glutaraldehyde for minimally 4 h at room temperature, and subsequently washed and stored with PBS with 0.1 mM $CaCl_2$ at room temperature. For embedding, the cells were pelleted and dehydrated in an alcohol series and embedded into epon resin. With an ultramicrotome the cells were sectioned in 70-200 nm coupes and collected onto formvar coated 200 Mesh copper grids (Fort Washington, PA, USA). The grids were contrasted for electron microscopy with uranyl acetate and counterstained with lead citrate. After staining the grids were imaged using a Tecnai 12 transmission electron microscope (1900× for 289B, 2900× for 081R, or 9300× magnification, 120 kV).

### Lentiviral knockdown and overexpression

Lentivirus was produced by transfecting HEK293T cells with either pLKO.1 targeting construct (see Key Resources for sequences) or scrambled non-targeting control shRNA (shc002) for knockdown experiments. For overexpression experiments, a pLeGO-V2 overexpression construct with an *ESRRA* ORF (ESRRA_OHu20547C) or a *PPARGC1A* ORF (PPARGC1A_OHu27412C) was used. Control was empty pLeGO-V2 control (#27340, Addgene[46]). To generate lentivirus, HEK293T cells were transfected with the above transfer plasmids, and packaging plasmids pMD2.G, pMDLg/pRRE, and pRSV-Rev using Lipofectamine 2000 (Invitrogen, Waltham, Massachusetts). Supernatant was harvested after 48 and 72 h and filtered through a 0.45 μm filter (Millipore, Germany). 081R and

289B cells were transduced at 70% confluency with the harvested virus in the presence of 8 μg/mL polybrene (Sigma) overnight. Two days after transduction knockdown cells were selected for stable transduction with 2 μg/mL puromycin (Sigma). Five days after transduction overexpression cells were sorted (Sony SH800, Tokyo, Japan) for Venus positivity.

### Luciferase 3xERRE reporter assay

HEK293T cells were seeded in 6-well plates at 2 × $10^5$ cells per well. The following day, cells were co-transfected with 3000 ng 3xERRE-luciferase construct,[19] and 600 ng of pRL-CMV-Renilla, respectively. After overnight incubation, transfection complexes were removed and the medium was replaced with regular DMEM medium. At 24 h post-transfection the cells were irradiated. At 48 h post-transfection, cells were lysed and analyzed for dual-luciferase activity using Dual-Luciferase Reporter Assay System (Promega, E1910) and luminescence was measured (Biotek).

### GFP 3xERRE reporter generation

The 3xERRE sequence was introduced in the FpG5 vector by GenScript (Leiden, the Netherlands).[19,45] The following sequence was inserted flanked by *BamHI* and *NheI*: 5′ gatccCGGACCTCAAGGTCACGTTCGGACCTCAAGGTCACGTTCGGACCTCAAGGTCAG GATCCg -3′. Lentivirus was produced as described in the section Lentiviral knockdown and overexpression. Following transduction, selection was done using hygromycin (200 μg/mL) and sorting for GFP positivity (Sony SH800, Tokyo, Japan).

### GFP 3xERRE reporter assay

3xERRE-GFP transduced cells were seeded in 24-wells culture plate (081R 1 × $10^5$, 289B 5 × $10^4$ cells/well). After 24 h, the cells were treated (irradiation or ROS-inducer) for 3 consecutive days. The following day, the cells were harvested and GFP fluorescence was measured on the FACS (BeckmanCoulter CytoFLEX-S, Brea, CA, USA). For the double transduced cells with pLEGO-iV2-PPARGC1A, 3xERRE-GFP cells were transduced with pLEGO-iV2-PPARGC1A or pLEGO-iV2 virus (see lentiviral knockdown and overexpression). After 72 h, the cells were analyzed on the spectral FACS (Sony SP6800, Tokyo, Japan).

### ESRRA ChIP qPCR

Following exposure to chemoradiation, cells were processed for pull-down according to the Cut-and-Run protocol and kit (Cell Signaling). Briefly, 4 × $10^5$ cells were harvested, washed, and bound to activated Concanavalin A-coated magnetic beads and permeabilized. The bead–cell complex was incubated overnight with the respective antibody at 4°C. Cells were washed two times and resuspended in 100 μL pAG/MNase and incubated for 30 min at 4°C. Input samples were obtained using the included DNA Extraction Buffer combined with sonification (100-600 bp fragment size). Antibodies used were against ESRRA (see key resources table, Ab76228, 1:20 dilution) and the included IgG control (1:20 dilution). Following pull-down, qPCR for SDHA was performed or an unrelated gene (*IKZF3*).[20] DNA input (2%) was taken along. PCR data were corrected for input, non-specific binding by control IgG and expressed as fold change relative to untreated controls.

### Immunofluorescence

Cells were seeded on glass coverslips in 12-well plates (per well 2 × $10^5$ 081R cells, 1 × $10^5$ 289B cells), to allow imaging and exposed to 1Gy for 72 h. Cells were washed twice with PBS, fixed using 4% formaldehyde in PBS for 10 min, washed again and permeabilized using 1% Triton X-100 in PBS. Blocking was done using 5% goat serum (NGS)/0.1% Triton X100/PBS for 30 min. Antibodies were incubated overnight at 4°C in blocking buffer at the following dilutions: anti-ESRRA at 1:100 dilution (Merck), anti-Beta-I tubulin at 1:100 (Sigma). After washing, secondary antibodies were added: Alexa 568 anti-mouse IgG1 and Alexa 488 anti-rabbit IgG (H+L), both 1:100 (Invitrogen). Hoechst was added 1:1000. After further washing, cells were mounted in Prolong Gold and imaged on an SP-8 confocal microscope (Leica).

### IncuCyte live cell imager

For cell confluence measurements, cells were plated in 96-well tissue plates (per well 1 × $10^5$ 081R cells, 5 × $10^4$ 289B cells). After 24 h, cells were washed and media was replaced with media containing indicated treatments. Photomicrographs were collected using the 10× objective with four planes of view per well at 72 h. Phase contrast images were collected, and confluence was calculated as percentage of surface. For competition measurements with *pLeGO-iV2-ESRRA*, cells were plated in 6-well tissue plates (per well 2 × $10^5$ 081R cells, 1 × $10^5$ 289B cells), treated with 14d chemoradiation or left untreated. Total confluence area of cells, and Venus positive and negative cell area were determined by Incucyte to determine proportional outgrowth. For apoptosis measurements, c ells were plated in standard 96-well tissue culture plates (per well 1 × $10^5$ 081R cells, 5 × $10^4$ 289B cells). After 24 h, cells were washed and media was replaced with media containing indicated treatments, and 1 μg/mL Annexin V ATTO 488 (Adipogen Life Sciences, Liestal, Switzerland). Photomicrographs were collected using the 10X objective with a single plate view per well. Phase contrast and green fluorescence channel (440/80nm–504/44 nm) images were acquired at 72 h. Annexin-positive area was calculated as total green object area (μ$m^2$/image).

### Multi-dose combination cell viability assay

Cells were plated in standard 96-well tissue culture plates (per well $1 \times 10^5$ 081R cells, $5 \times 10^4$ 289B cells). After 24 h ESRRAi LP0821 was added by HP D300 digital dispenser. After an additional 72 h, cells were washed with PBS, fixed with 1% glutaraldehyde and 0.5% crystal violet. After 20 min incubation at RT, cells were immersed in tap water and air-dried. Pictures were made on a digital scanner (HP Scanjet 4850). Subsequently, crystal violet was dissolved overnight with 1% SDS and absorbance was measured at 600 nm (Biotek). Absorbance values were subtracted by background absorbance and normalized to control conditions. ZIP-score was calculated and synergy landscape was generated by the *synergyfinder* R package.

### Cell viability 3D culture

For the proliferation assay, EAC organoids were seeded with 150 single cells in 6μL Matrigel per well. The first 72 h (day −3 to 0), the medium was supplemented with ROCK inhibitor (Y-27632). For the rest of the assay, standard organoid medium was used without NAC. This medium was provided on day 0 and 4. ESRRAi concentration and radiation dosages are indicated in Figure 5. ESRRAi was only present in the culture medium between day 0 and day 4. Radiation was also given in this time period on a daily basis.

For the clonogenicity assay, EAC organoids were seeded with 150 single cells in 6μL Matrigel per well. The first 72 h (day −3 to 0), the medium was supplemented with ROCK inhibitor. For the remainder of the assay, standard organoid medium was used and was refreshed every 3–4 days. 20μM ESRRAi was added at the indicated conditions and was supplemented directly before medium refresh. Daily radiation (1Gy) was given for the indicated conditions. On day 14, Matrigel was dissolved using Cell Recovery Solution (Corning) following manufacturer's instructions and organoids were split by mechanical disruption. Organoids were then transferred to a 48-wells plate in a 20μL Matrigel droplet and cultured for 7 more days without any treatment. Cell viability was quantified by image-analysis using the nuclear dye Hoechst (10 μg/mL, ThermoFisher). Hoechst was added to the culture medium for 15 min and washed away. Organoids were subsequently imaged by ImageXpress Pico (Molecular Devices, San Jose, CA, USA) automatic fluorescence microscope using a 4× magnification. Organoid surface area was quantified using QuPath's pixel classifier. Organoid count was quantified by using ImageJ.

### RNA-sequencing

Snap frozen tumor biopsy samples were collected before and after chemoradiotherapy under ethical approval (BiOES biobank; METC 2013_241) and 20 μm slices were cut on a cryostat. One section was used for haematoxylin and eosin staining to determine tumor cell percentage. Assessment of tumor purity was done by an experienced pathologist (SLM). Of 139 assessed esophageal biopsies and 105 resections, median tumor cellularity was 45 and 35%, respectively. Samples were considered eligible in case tumor purity was $\geq$ 30%. Matched pre- and post-treatment samples were identified for 6 patients. Total RNA was isolated using the AllPrep DNA/RNA/miRNA universal kit (Qiagen, Hilden, Germany). NanoDrop (Thermo Fisher, Waltham, MA) was used to measure RNA concentration. Biopsies and resection specimens were sent for RNA sequencing in case RNA concentration was above 20 ng/μL. Library preparation was performed using Total RNA library prep RiboErase (Roche, Basel, Switzerland). Samples were sequenced on an Illumina HiSeq4000 with single 50 bp reads at 100M reads per sample.

### Immunohistochemistry

Biopsies and resection specimens from 17 patients were fixed in 4% formalin overnight prior to paraffin embedding. Tissue sections (5 μm) were deparaffinized and antigen retrieval was performed using 10 mM sodium citrate and boiling for 20 min. Endogenous peroxidase activity was blocked with 3% hydrogen peroxide in PBS. Aspecific staining was blocked using UltraVision Protein Blk (Thermo Scientific, Waltham, MA) 10 min on RT. Primary antibody anti-COX4 (3E11 Rabbit mAb 4850, Cell Signaling, Danvers, MA) was diluted 1:3000 diluted in BrightDiluent green antibody diluent (Immunologic, Duiven, The Netherlands), and incubated overnight at 4°C in a humidified chamber. For amplification of the staining, Brightvision+ post antibody block (Immunologic, Duiven, The Netherlands) was used for 20 min prior to the addition of the secondary antibody, poly-HRP-anti Ms/Rb IgG (Immunologic, Duiven, The Netherlands) for 30 min at RT. Visualization of stainings was performed with Bright DAB solution (Immunologic, Duiven, The Netherlands) according to manufacturer's protocol, counterstained with undiluted Mayer Haematoxylin (Klinipath, Duiven, The Netherlands) and mounted tissue sections with non-aqueous medium. Slides were assessed by a trained pathologist to identify tumor areas. Fibroblasts and extracellular matrix were excluded and the remaining tumor ROIs were assessed for COX4 intensity using the Immunohistochemistry (IHC) plugin from Image Analysis Toolbox in ImageJ.

### Quantitative PCR

Genomic DNA isolation was performed using QuickExtract Extraction Solution (Lucigen, Middleton, USA) according to the manufacturer's protocol. RNA was isolated according to manufacturer's instructions (Macherey-Nagel, Duren, Germany). Subsequently, cDNA was synthesized with Superscript III, DTT, 5× First-Strand Buffer, RNAseOUT and dNTP Mix (Thermo Scientific, Waltham, MA) according to the manufacturer's protocol. SYBR green (Roche, Basel, Switzerland) was used to perform quantitative real-time PCR (qPCR) on a Lightcycler 480 II (Roche) according to manufacturer's instructions. For primer sequences, see key resources table.

### Seahorse XF-96 metabolic flux analysis

The Seahorse XF96 Extracellular Flux Analyzer (Seahorse Biosciences, Santa Clara, California, USA) was used to obtain real-time measurements of oxygen consumption rate (OCR) and extracellular acidification rate (ECAR) in cells. Cells were seeded in 96-well Seahorse culture plates at a density between 25,000 and 50,000 cells/well and were reconstituted in culture medium overnight. Prior to the analysis, the culture medium was replaced with Assay Medium; DMEM at 25 mM glucose, sodium pyruvate 1 mM and L-glutamine 2 mM. Concentrations were according to the manufacturer's instructions. Assay medium was subsequently adjusted to pH 7.4 and maintained at 37°C throughout the experiment. For the "Mito Stress Test" protocol oligomycin (1.5 μM), FCCP (1 μM), and Antimycin A (2.5μM) and Rotenone (1.25 μM) were sequentially injected according to the manufacturer's instructions. All values were normalized by protein abundance assessed a BCA assay kit.

### Flow cytometry

To assess mitochondrial mass by flow cytometry (FACS), cells were harvested with trypsin-EDTA (Lonza, Basel, Switzerland) and stained with 50 nM MitoTracker Deep Red FM (Thermo Scientific, Waltham, MA) for 30 min at 37°C. Cells were washed in FACS buffer (PBS with 1% FCS) prior to flow cytometry analysis. For flow cytometric detection of ROS production, cells were harvested as above, and stained with 25 μM H2DCFDA (Thermo Scientific, Waltham, MA) for 1 h at 37°C. 3 mM $H_2O_2$ was used as positive control and treated for 1 h at 37°C before staining with H2DCFDA. For membrane potential assessment, cells were treated with 2 μM JC-1 for 30 min 20 μM FCCP was used as positive control and cells were treated for 1 h at 37°C before staining with JC-1. All samples were acquired on a FACSCanto II (BD, Franklin Lakes, NJ), measured at excitation 488 or 525 nm. Data were analyzed using FlowJo 10 (Tree Star, Ashland, OR). Ratio was calculated by dividing the gMFI of PE by the gMFI of FITC.

### *In vivo* radiation and ESRRAi

Three weeks after cell injection mice were treated for two consecutive weeks with or without 2 Gy of radiation (10 × 4Gy, 40Gy cumulative) on the right hind limb using an X-Ray RS320 Research Cabinet (XStrahl, 0.5 mm Cu filter, 210 kV, 13mA). The mice were shielded with lead to protect all other vital areas. Vehicle control (10% DMSO, 20% Solutol, 70% water) or ESRRAi LP0811 (30 mg/kg) were administrated by daily oral gavage in a volume of 100μL.

## QUANTIFICATION AND STATISTICAL ANALYSIS

### RNA-sequencing analysis

Data went through quality control using FastQC. Reads were aligned to the human reference genome (NCBI37/hg19) using STAR v2.7.1 and annotated with Gencode v32. For gene set enrichment, count files were converted into DESeq2_vst values using DESeq2 in R. Differential gene expression between pretreatment biopsies and posttreatment resection material was determined by using the limma R package. Gene set enrichment analysis was performed on using all Hallmark gene sets[52] using the subcamera function of CMScaller,[47] and fGSEA (http://bioconductor.org/packages/fgsea/).[48] *ESRRA* target genes were derived from Stein et al.[18] Upregulated targets genes were selected by *Class 1* and $p < 0.01$, and downregulated target genes were selected by *Class 5* and $p < 0.01$.

### Gene expression correlated to OxPhos signature

Signature scores were calculated for the OXPHOS signature (Table S6) as follows: Every gene was transformed by Z-score across all the samples in the cohort shown (Figure 3; including all adenocarcinoma samples). Then per sample, the list of OXPHOS genes was summarized into a single value by calculation of the average over all OXPHOS genes. The signature scores were subsequently used to calculate the Pearson correlation against all the genes in the dataset. The significance of a correlation is determined by t = R/sqrt((1-r∧2)/(n-2)), where R is the correlation value and n is the number of samples. Distribution measure is approximately as t with n-2 degrees of freedom. The p values reported are False Discovery Rate (FDR) adjusted, plotted as the negative log10 values. Dots indicate genes.

### Statistical analysis

To compare two means, a two-tailed Student's t test was used. When data were not normally distributed a Mann-Whitney U test was performed. To compare multiple groups of data to one control condition and when the data is not normally distributed, we performed a Kruskal-Wallis test. Survival analysis was performed by Log Rank Mantel-Cox test. The performed statistical tests are also indicated in the figure legends. Analyses were performed by Prism 9 (Graphpad Software Inc., version 9.3.1) or in R. A $p < 0.05$ was considered statistically significant. *$p < 0.05$, **$p < 0.01$, ***$p < 0.001$, ****$p < 0.0001$.